

Experimental X-Ray Spectroscopy: Part 1

John Seely, seelyjf@gmail.com

Outline:

- X-ray spectrometer optical design and capabilities:
 - Reflection crystals (Bragg)
 - Transmission crystals (Laue, Cauchois)
- Experiments at large laser and other facilities and example results.

Science Motivation:

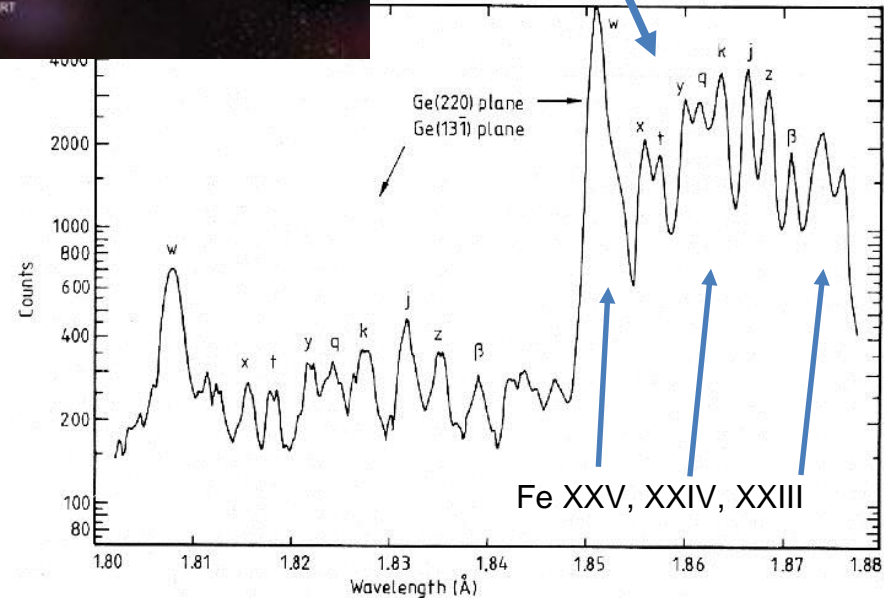
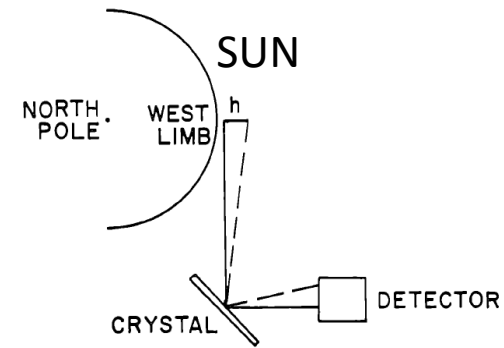
- Atomic physics of inner-shell transitions in high atomic number atoms and highly charged ions.
- High-energy-density (HED) plasma diagnostics: temperature, density, ionization balance, opacity.
- Atomic physics code validation (FAC, HULLAC, FLYCHK, opacity, ...)
- Atomic kinetics code validation (FLYCHK, NOMAD, ...)

X-ray spectroscopic plasma diagnostics provide:

- **Identification of bound-bound transitions**
 - Measurement of transition energies (atomic physics code validation)
 - Determination of ionization balance (kinetics code validation)
- **Measurement of spectroscopic line ratios**
 - Electron temperature and density, opacity
- **Measurement of continuum emission**
 - Bound-free transition opacities; super-thermal electron energy component
- **Measurement of line widths, line shapes, energy shifts**
 - Doppler broadening, Stark broadening, opacity (requires high spectral resolution)
- **Spectra with temporal and/or spatial resolution**
 - Transient dynamics
- **Measurement of absolute intensities**
 - Source brightness, laser energy to x-ray conversion efficiency (Inertially Confined Fusion, ICF)
 - Density

Many Sources of X-Rays

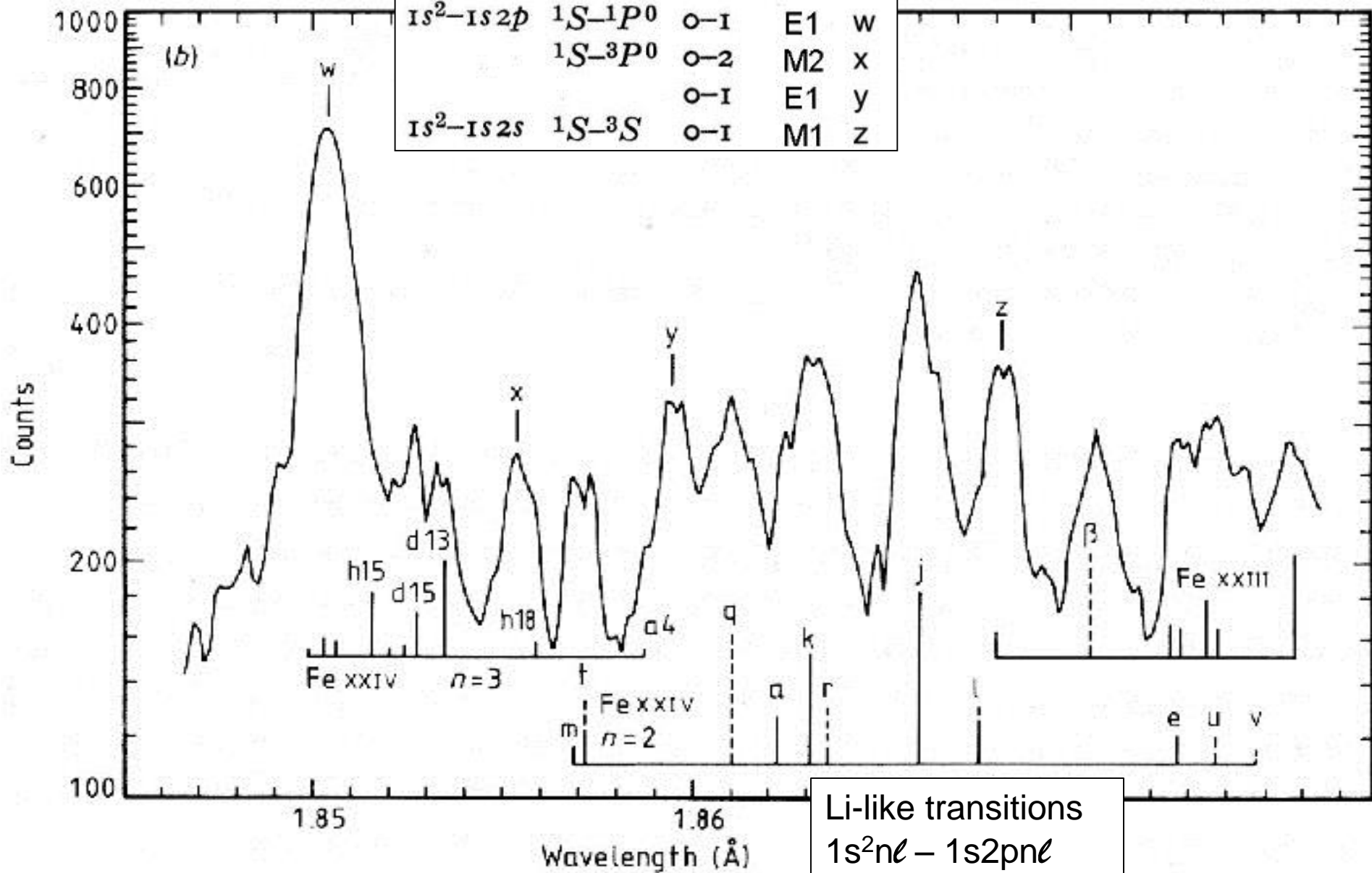
- Astrophysical
- Solar flares
- Low-density laboratory
 - Tokamaks
 - Electron Beam Ion Trap (EBIT)
- High-density laboratory
 - **Long-pulse laser (ns)**
 - **Short-pulse laser (ps and fs)**
 - **Pulsed-power generators**
- X-ray free electron lasers (XFEL): FLASH, **LCLS**, European XFEL, up to 25 keV
- Laboratory testing and calibrations
 - **Laboratory electron-bombarded anode (W, 300 kV at NIST)**
 - Radioactive sources (x-rays, gamma rays)



Solar Flare X-Ray Spectrum

He-like transitions

| | | | | |
|-------------|-----------|-----|----|---|
| $1s^2-1s2p$ | $1S-1P^0$ | o-1 | E1 | w |
| | $1S-3P^0$ | o-2 | M2 | x |
| $1s^2-1s2s$ | $1S-3S$ | o-1 | E1 | y |
| | | o-1 | M1 | z |



Reflection and Transmission Crystal X-Ray Spectrometers

$n\lambda = 2d \sin\theta$ (Bragg condition) where
 n = diffraction order (usually $n=1$)
 λ = wavelength ($E = hc/\lambda$, usually > 1 keV)
 d = crystal lattice spacing (few nm)
= distance between diffracting planes
 θ = Bragg angle
= grazing angle to diffracting planes

Bragg case:

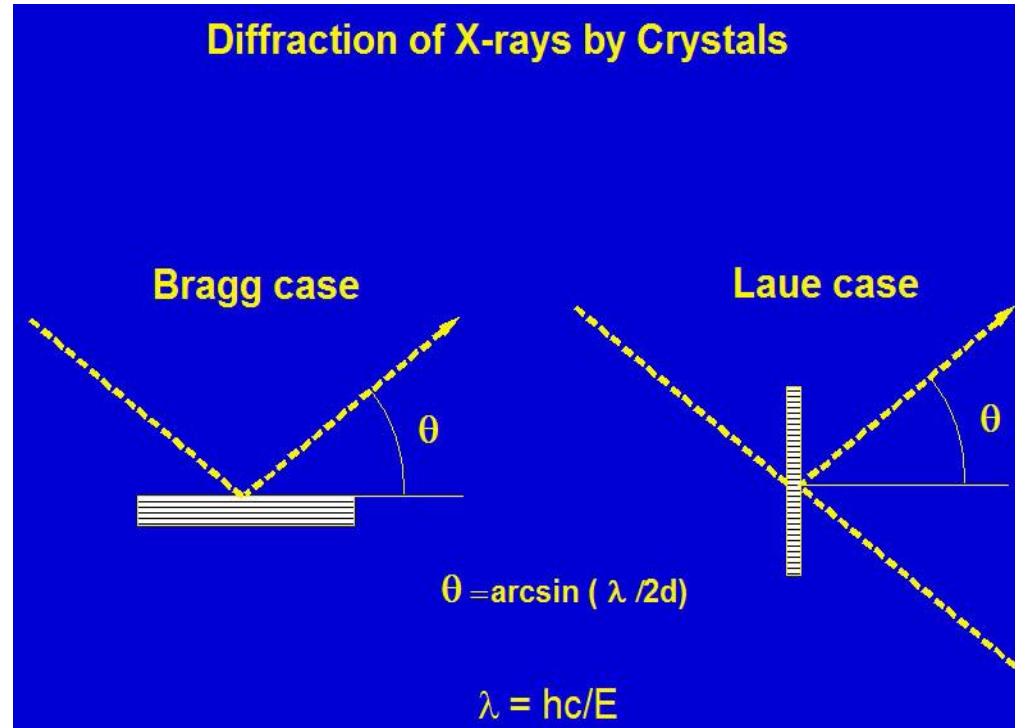
Diffracting planes are parallel to crystal surface
Larger angles (> 10 of deg)
Lower energies (< 10 keV)

Laue case:

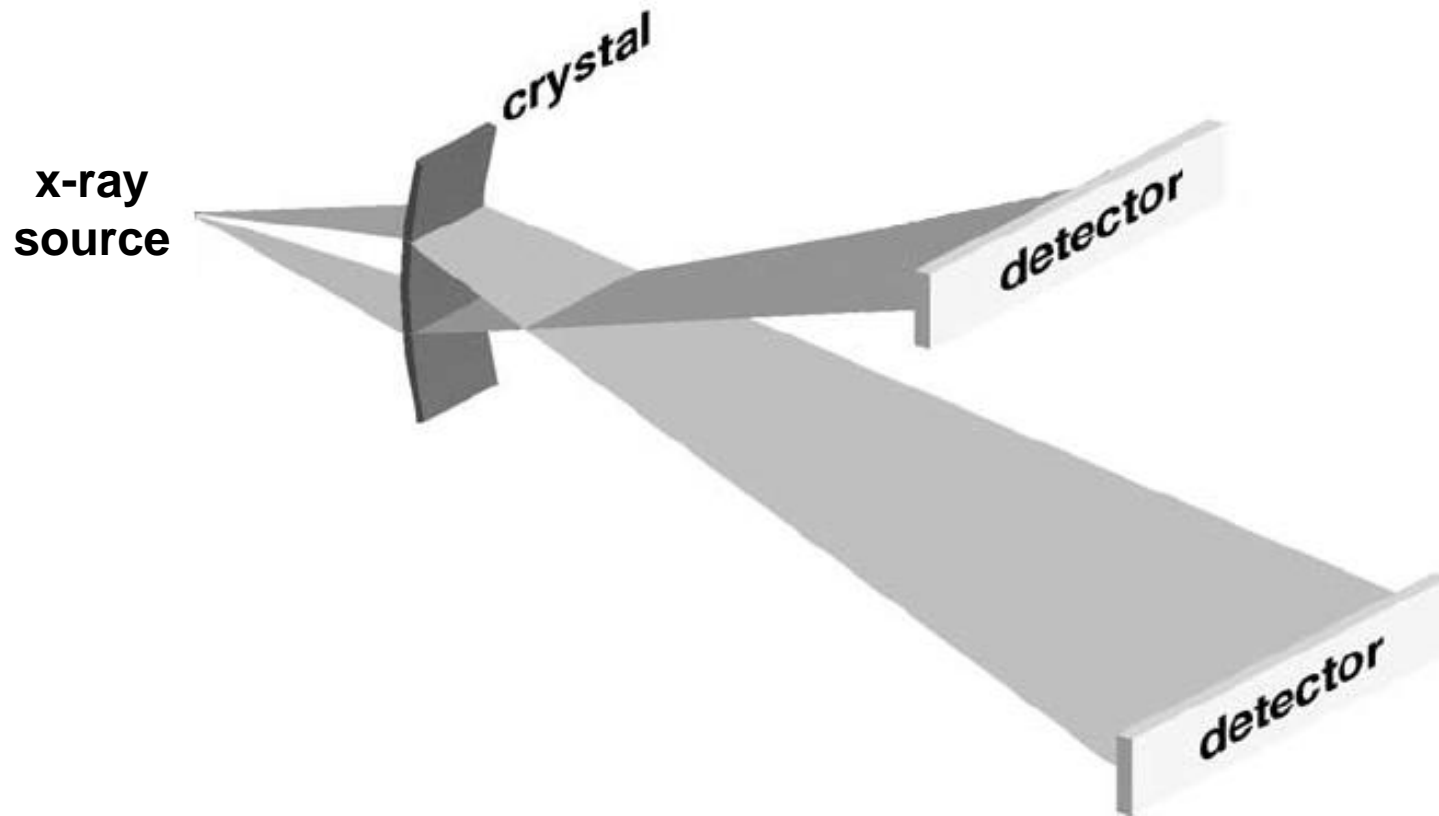
Diffracting planes perpendicular to crystal surface.
Smaller angles (< 10 deg)
Higher energies (> 10 keV)

Bending:

- Concave facing the x-ray source (narrower angle and energy ranges, spatial resolution)
- Convex facing the x-ray source (broader angle and energy ranges)
- Single bending (e.g. cylindrical)
- Double bending (e.g. spherical, conical)

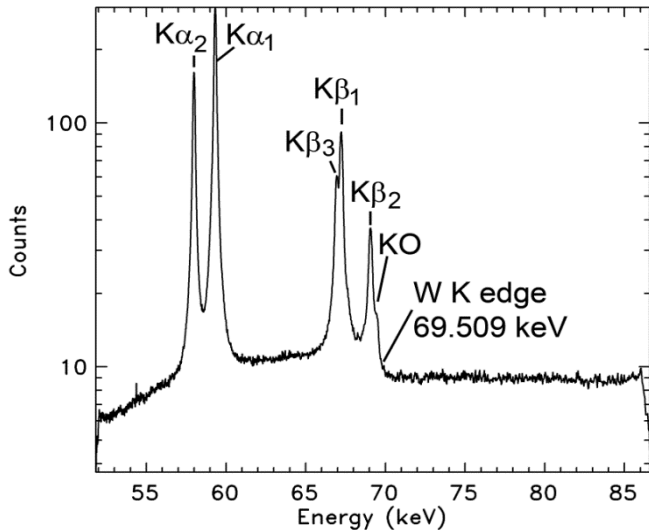
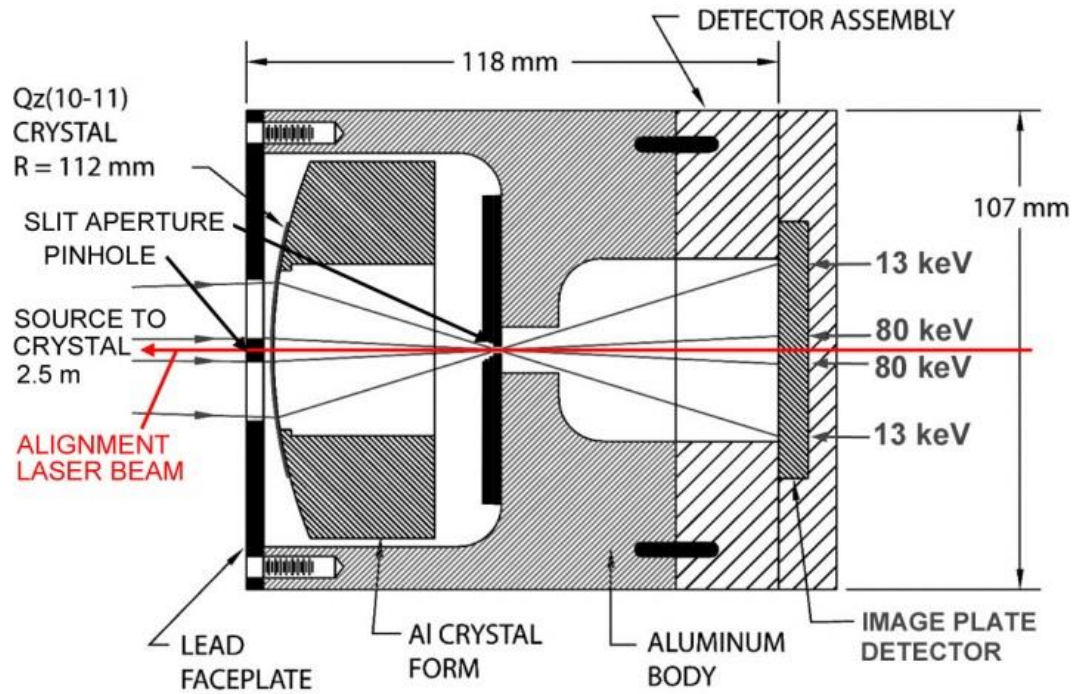


Transmission Crystal Spectrometer (Cauchois, 1932)

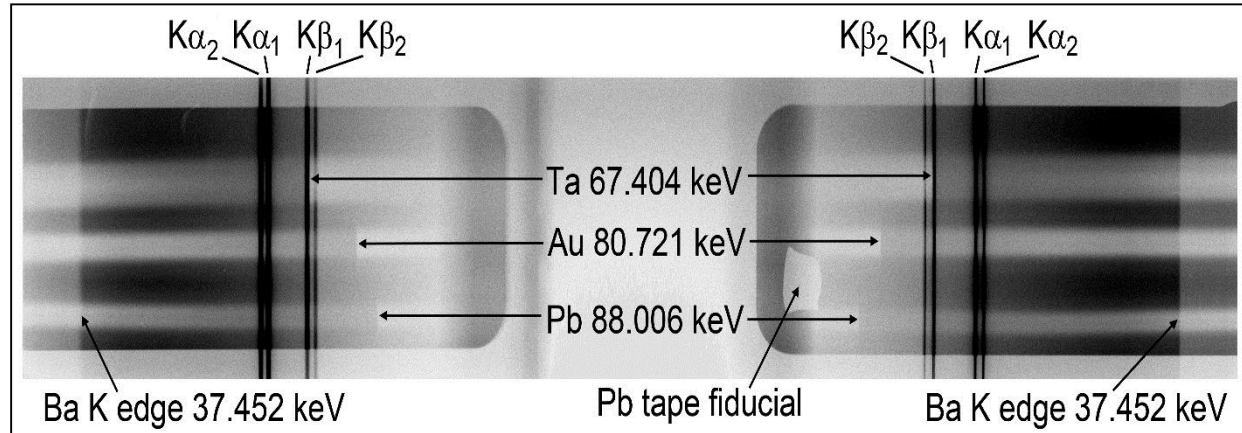


- Cylindrically bent crystal with convex side facing the x-ray source.
- All rays with the same energy and from an extended source are focused on the Rowland circle (diameter equal to the radius of the crystal). **No source size broadening.**
- Rays with different energies are dispersed on the Rowland circle.

Transmission Crystal Hard X-Ray (> 10 keV) Spectrometer



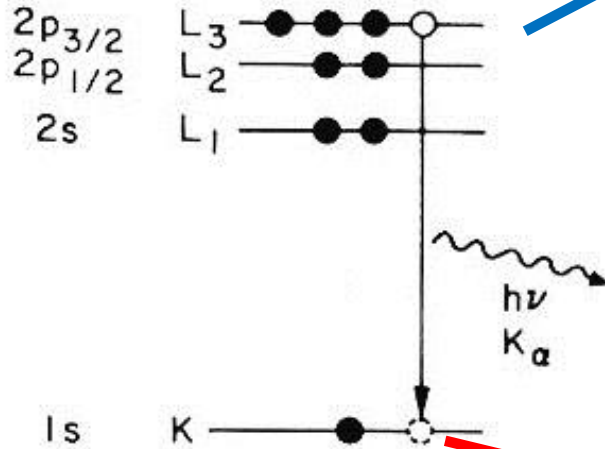
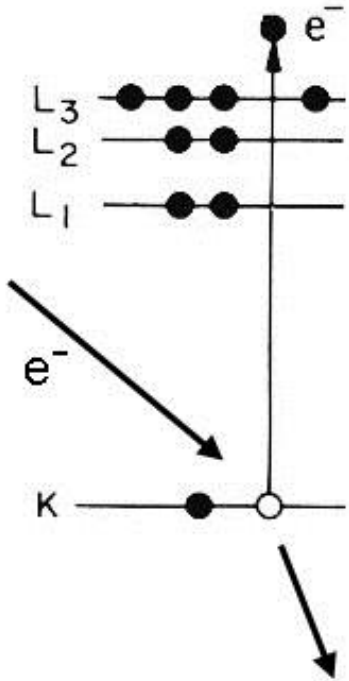
Spectrum from an electron-bombarded W anode



Energetic Electrons (and Photons) \rightarrow 1s Vacancies \rightarrow X-Ray Spectra

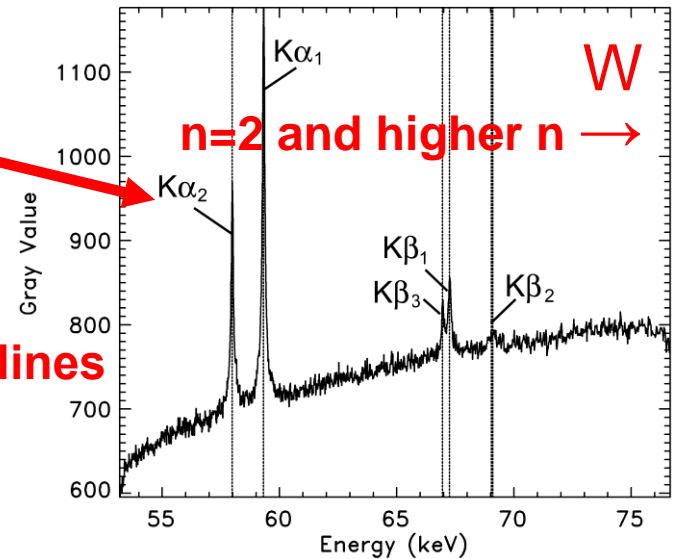
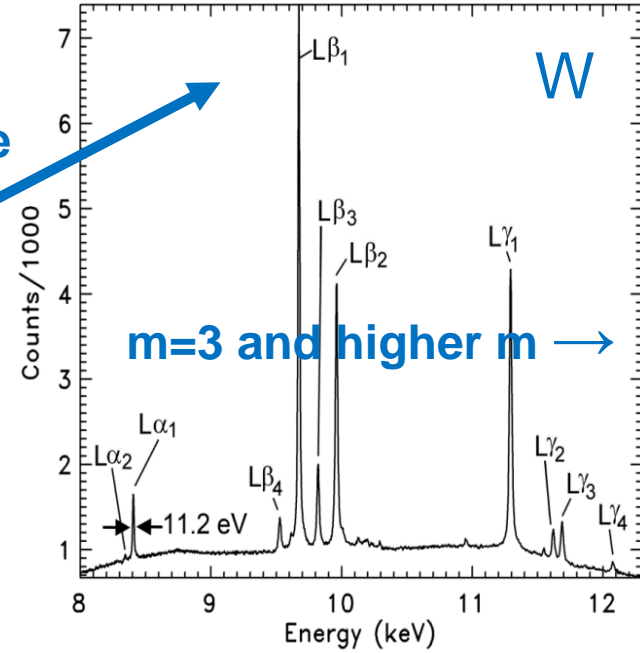
$n = 2$ vacancy

$m \rightarrow 2$ transition L spectral line

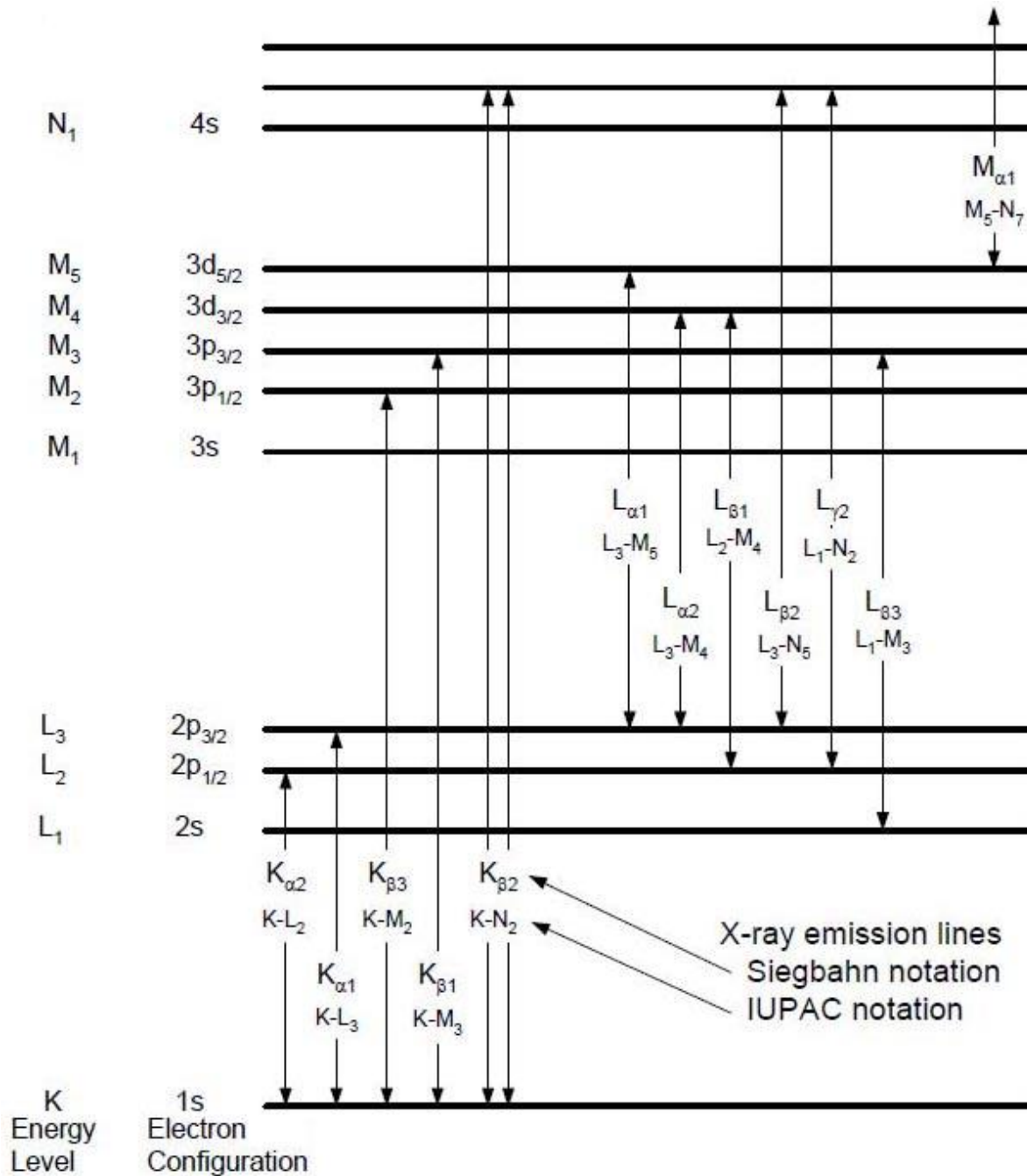


1s vacancy

$n \rightarrow 1s$ transition K spectral lines



Designations of Characteristic X-Ray Lines



Energies and intensities of W L Lines

| | | W L Transitions | | |
|----------------|--------|--------------------------------------|------------|-----------|
| Identification | Levels | Transition | Energy(eV) | Intensity |
| L α 2 | L3M4 | 2p _{3/2} -3d _{3/2} | 8335.3 | 11.22 |
| L α 1 | L3M5 | 2p _{3/2} -3d _{5/2} | 8398.2 | 100.00 |
| L η | L2M1 | 2p _{1/2} -4s _{1/2} | 8724.4 | 1.17 |
| L β 4 | L1M2 | 2s _{1/2} -3p _{1/2} | 9525.2 | 3.56 |
| L β 6 | L3N1 | 2p _{3/2} -4s _{1/2} | 9608.2 | 1.10 |
| L β 1 | L2M4 | 2p _{1/2} -3d _{3/2} | 9672.6 | 55.60 |
| L β 3 | L1M3 | 2s _{1/2} -3p _{3/2} | 9818.9 | 5.05 |
| L β 2 | L3N5 | 2p _{3/2} -4d _{5/2} | 9964.1 | 22.72 |
| L β 7 | L3O1 | 2p _{3/2} -5s _{1/2} | 10129.2 | 1.61 |
| L β 5 | L3O5 | 2p _{3/2} -5d _{5/2} | 10200.4 | 0.50 |
| L β 9 | L1M5 | 2s _{1/2} -3d _{5/2} | 10290.7 | 0.10 |
| L γ 5 | L2N1 | 2p _{1/2} -4s _{1/2} | 10948.9 | 0.10 |
| L γ 1 | L2N4 | 2p _{1/2} -4d _{3/2} | 11286.0 | 10.45 |
| L γ 6 | L2O4 | 2p _{1/2} -5d _{3/2} | 11538.7 | 0.40 |
| L γ 2 | L1N2 | 2s _{1/2} -4p _{1/2} | 11610.5 | 1.10 |
| L γ 3 | L1N3 | 2s _{1/2} -4p _{3/2} | 11680.5 | 1.61 |
| L γ 11 | L1N5 | 2s _{1/2} -4d _{5/2} | 11861.9 | 0.10 |
| L γ 4 | L1O3 | 2s _{1/2} -5p _{3/2} | 12063.4 | 0.10 |

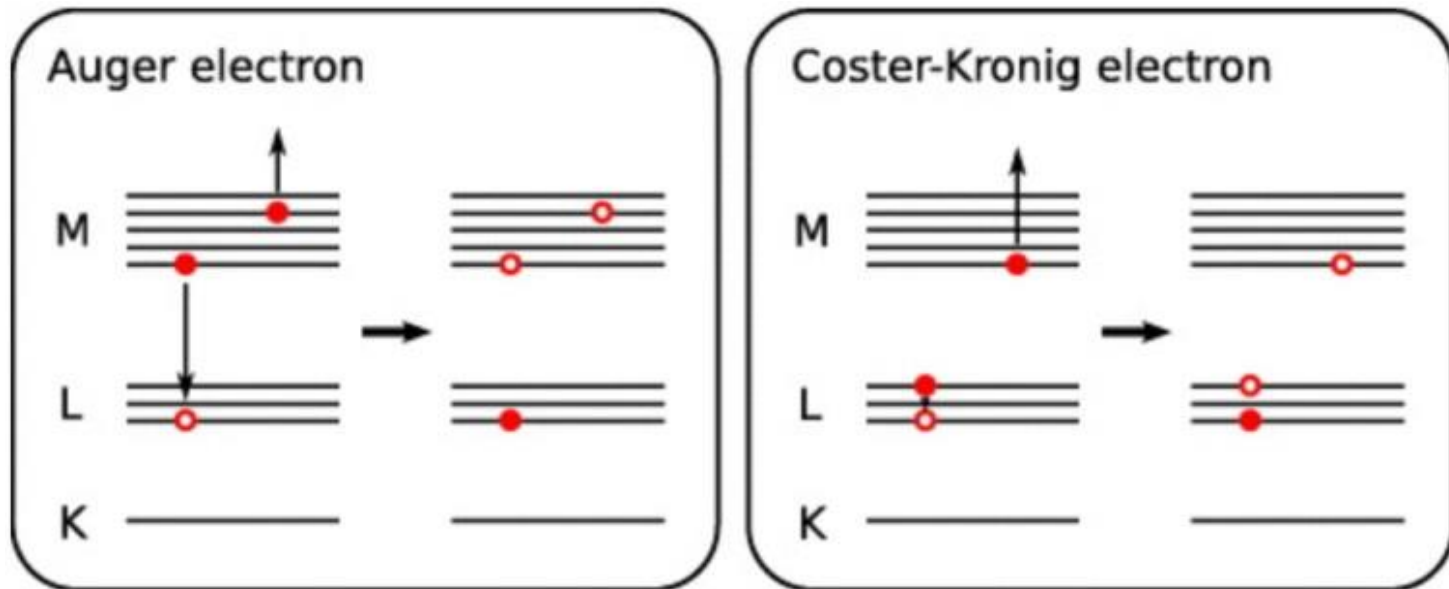
Energies of the characteristic x-ray transitions (type K, L, M, N) are very well known to a fraction of an eV (R. Deslattes, Rev. Mod. Phys. vol. 75, p. 35, 2003)

The lifetimes of the upper and lower levels contribute to the observed spectral lines widths (lifetime or natural widths).

Widths of the K transitions are dominated by the radiative decay rates: $\Delta E = (h/2\pi) A$

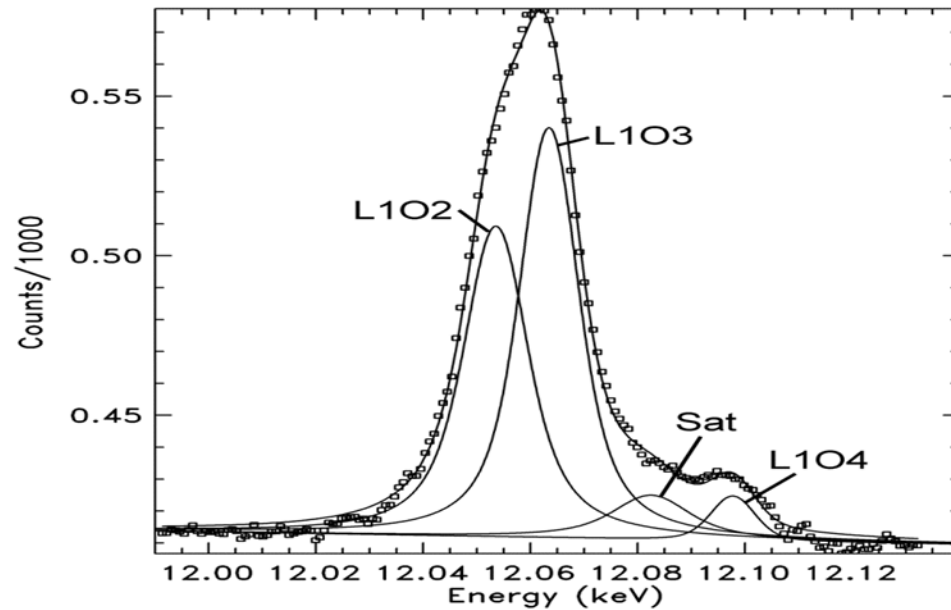
Widths of the upper levels of the L transitions are dominated by non-radiative rates:

Auger and Coster-Kronig



Line Widths are Measured by Fitting Voigt Profiles to the Ly4 Transition

Convolution of Gaussian and Lorentzian profiles.

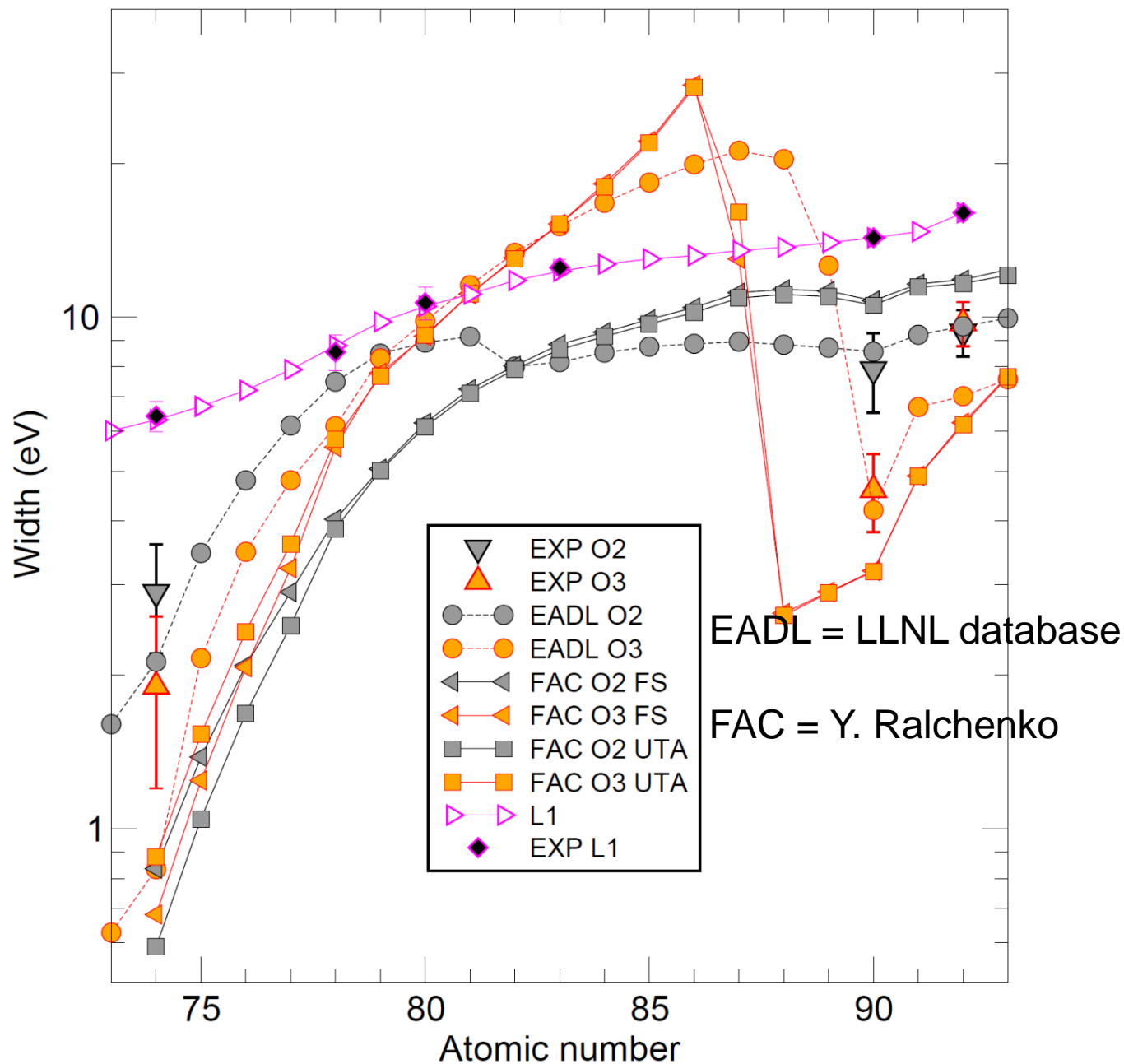


| | L1O2 (2s _{1/2} - 5p _{1/2}) | | L1O2 (2s _{1/2} - 5p _{3/2}) | |
|--|---|------------------|---|------------------|
| | Gaussian (eV) | Lorentzian (eV) | Gaussian (eV) | Lorentzian (eV) |
| Bent crystal broadening | 7.6 ± 0.5 | | 7.6 ± 0.5 | |
| Detector resolution | 2.8 ± 0.5 | | 2.8 ± 0.5 | |
| Experimental width | | 9.3 ± 0.3 | | 8.3 ± 0.3 |
| L1 (2s_{1/2}) natural width | | 6.4 ± 0.4 | | 6.4 ± 0.4 |
| Coster-Kronig width | | 2.9 ± 0.3, ± 0.4 | | 1.9 ± 0.3, ± 0.4 |

Coster-Kronig rates are determined from the widths.

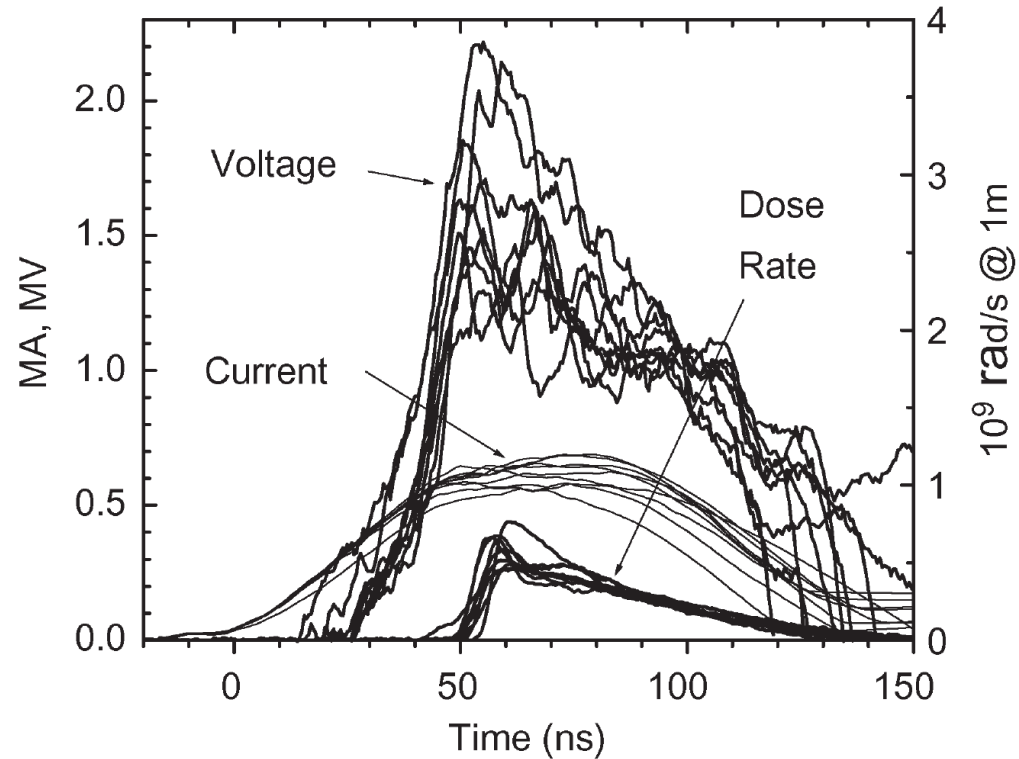
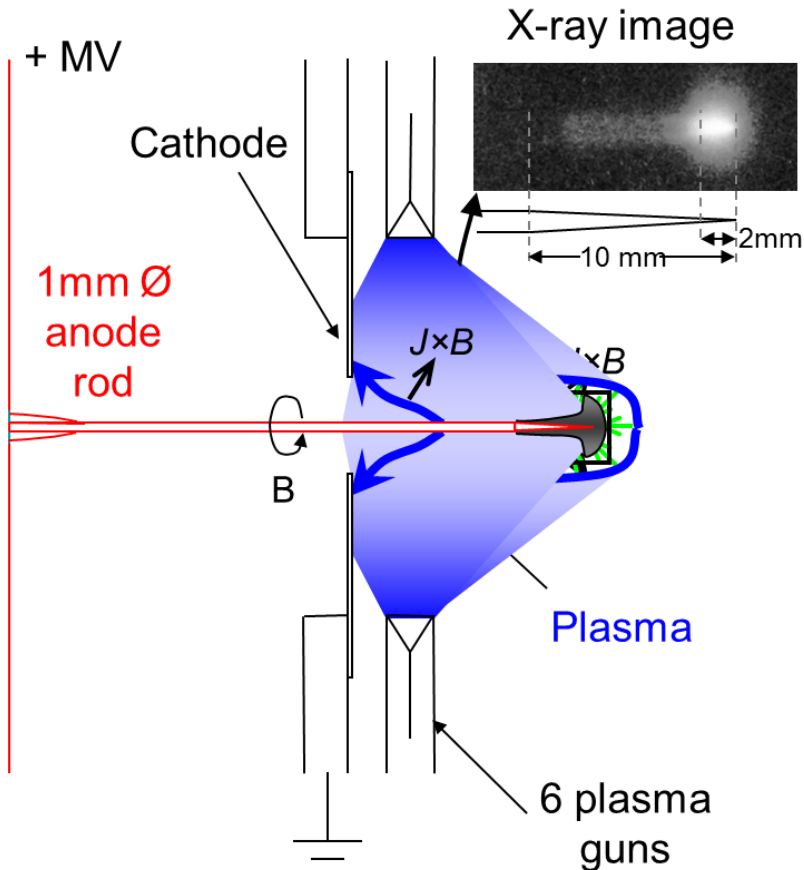
| Coster-Kronig process | O2O3O4 | O3O4O5 |
|------------------------------|---------------|---------------|
| Lifetime | 0.23 fs | 0.35 fs |
| Rate | 4.4e15 1/s | 2.9e15 1/s |

O2 ($5p_{1/2}$) and O3 ($5p_{3/2}$) Level Widths



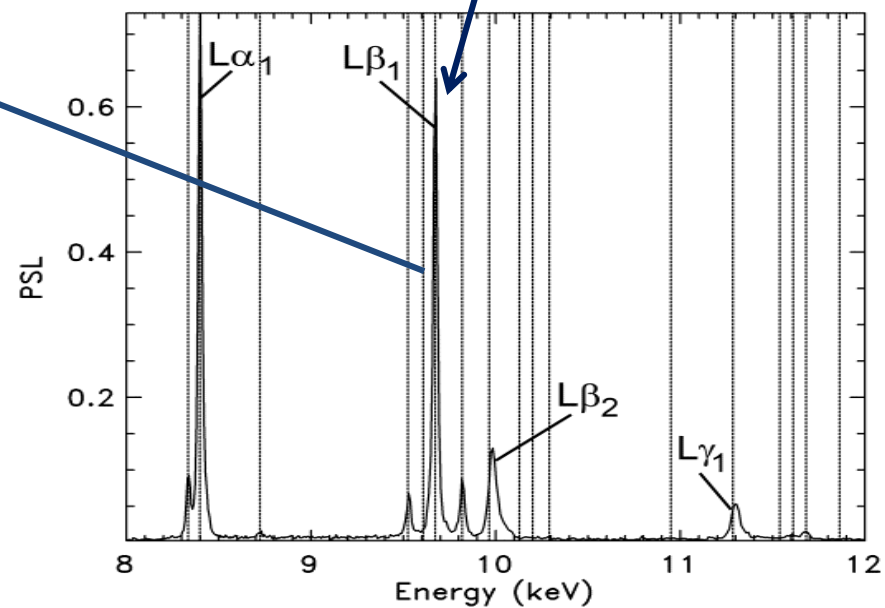
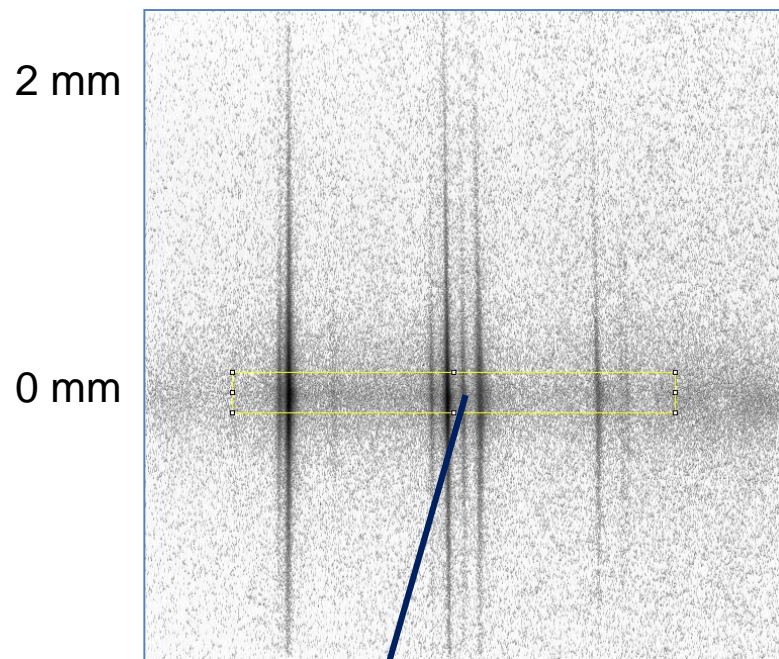
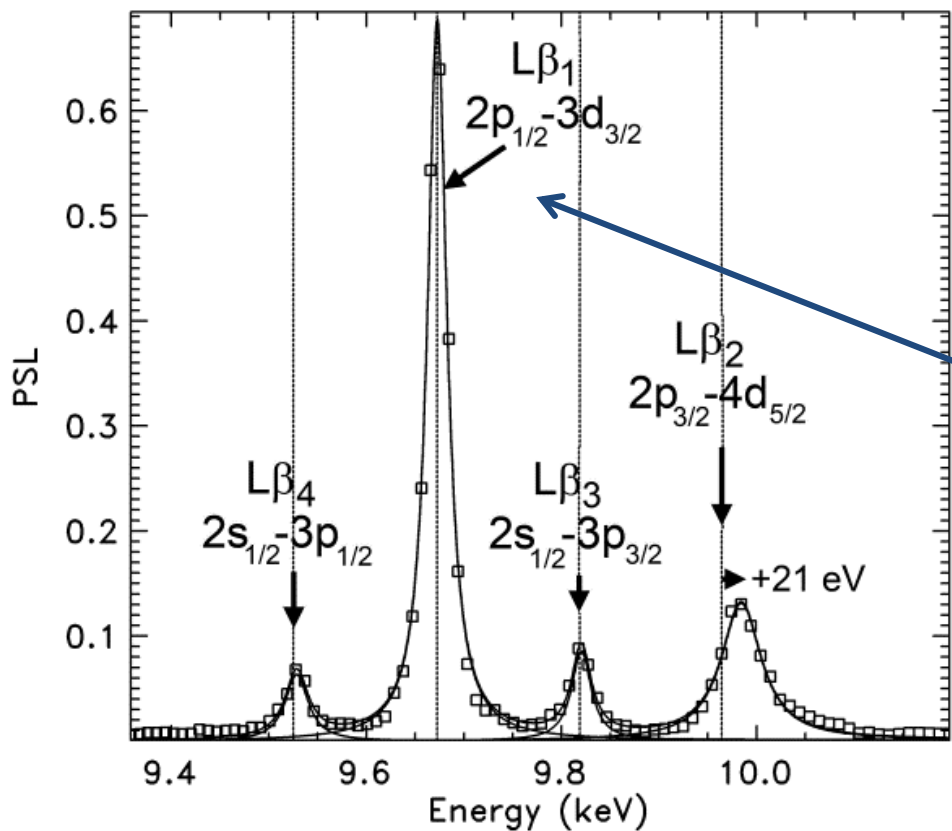
Pulsed Power X-Ray Generator of Warm Dense Plasma

Electron current: 2 MeV, 0.6 MA, 50 ns



W $L\beta_2$ line is broad, asymmetric, and shifted to higher energy by ionization

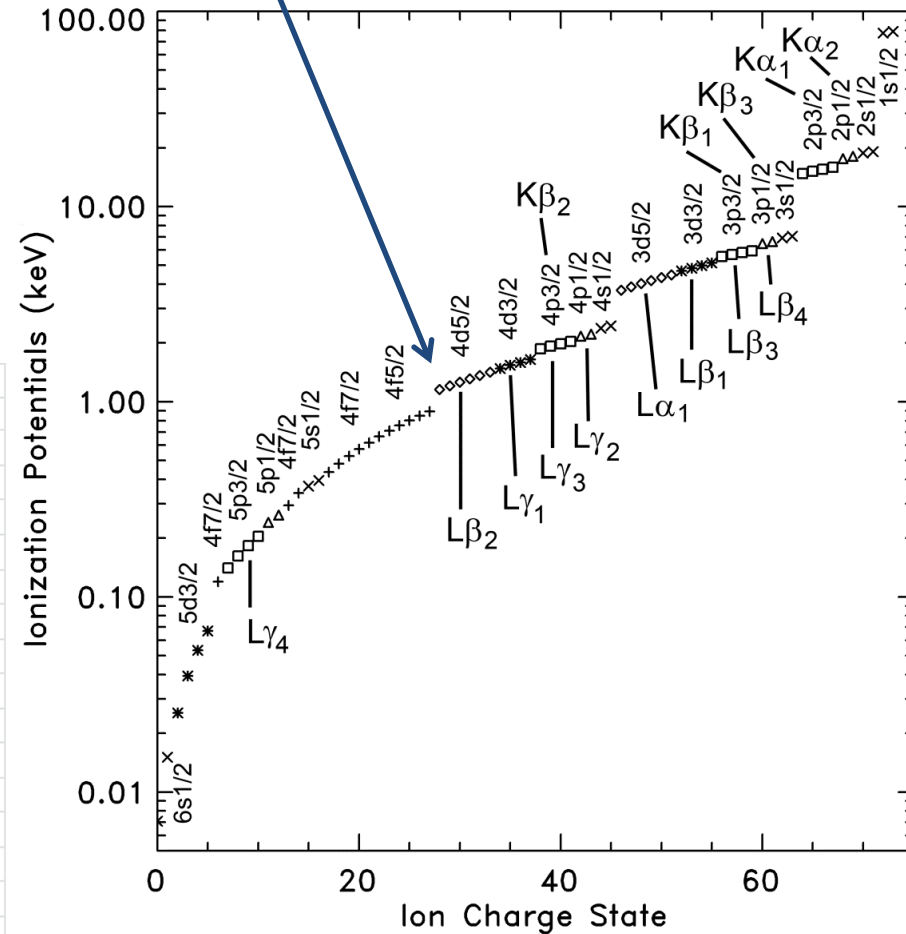
Vertical lines are characteristic transition energies:



$L\beta_2$ Transition is Shifted by Outer-Shell Ionization

- Ionization of the outer $6s^2$, $5d^4$, $5p^6$, $5s^2$, and $4f^{14}$, up to the +28 charge state and approaching the $4d^{10}$ Kr-like closed shell.
- $L\beta_2$ transition having $4d_{5/2}$ upper level is perturbed to higher energy.
- Other nearby $L\beta$ transitions from more tightly-bound $n=3$ levels are essentially unperturbed.

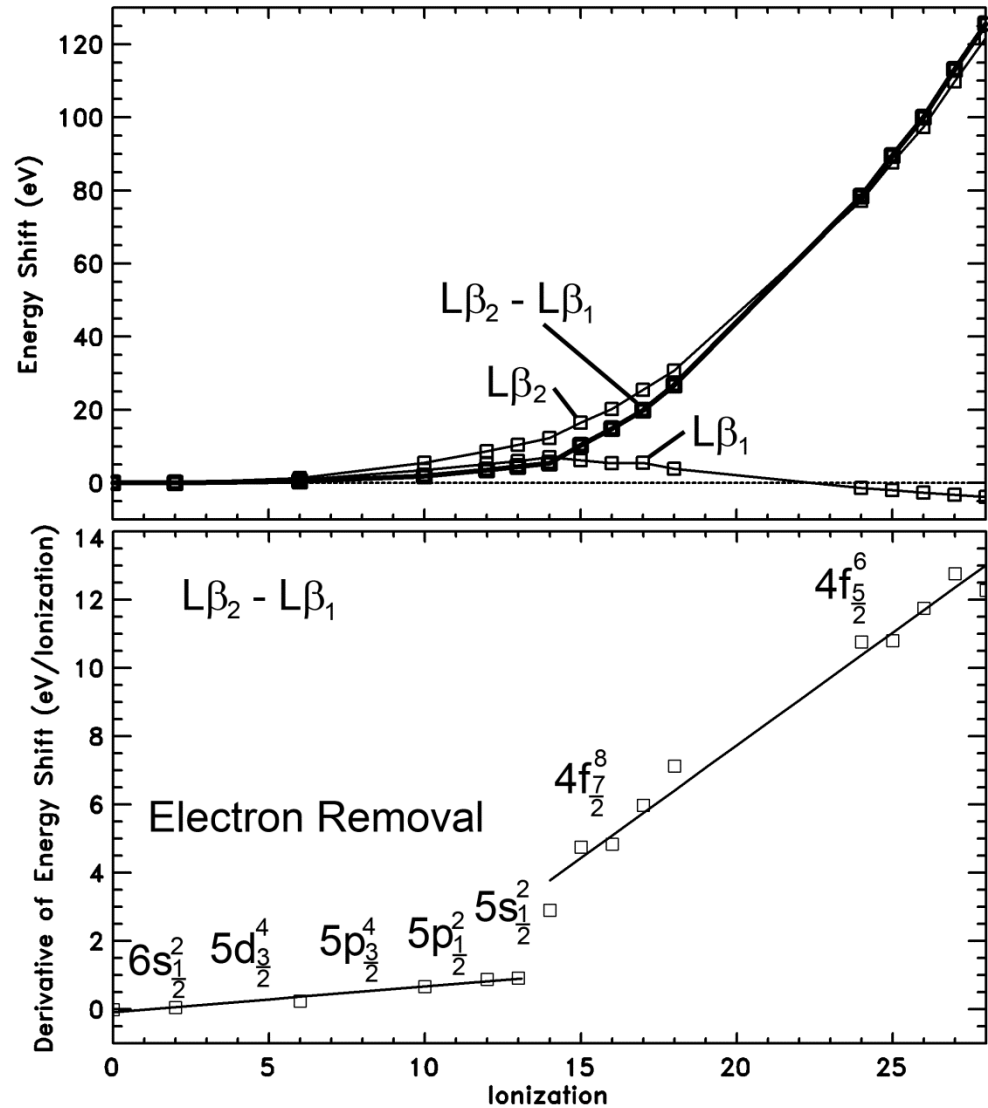
Ionization potential jump at the $[Kr]4d^{10}$ closed shell, $Z=28$



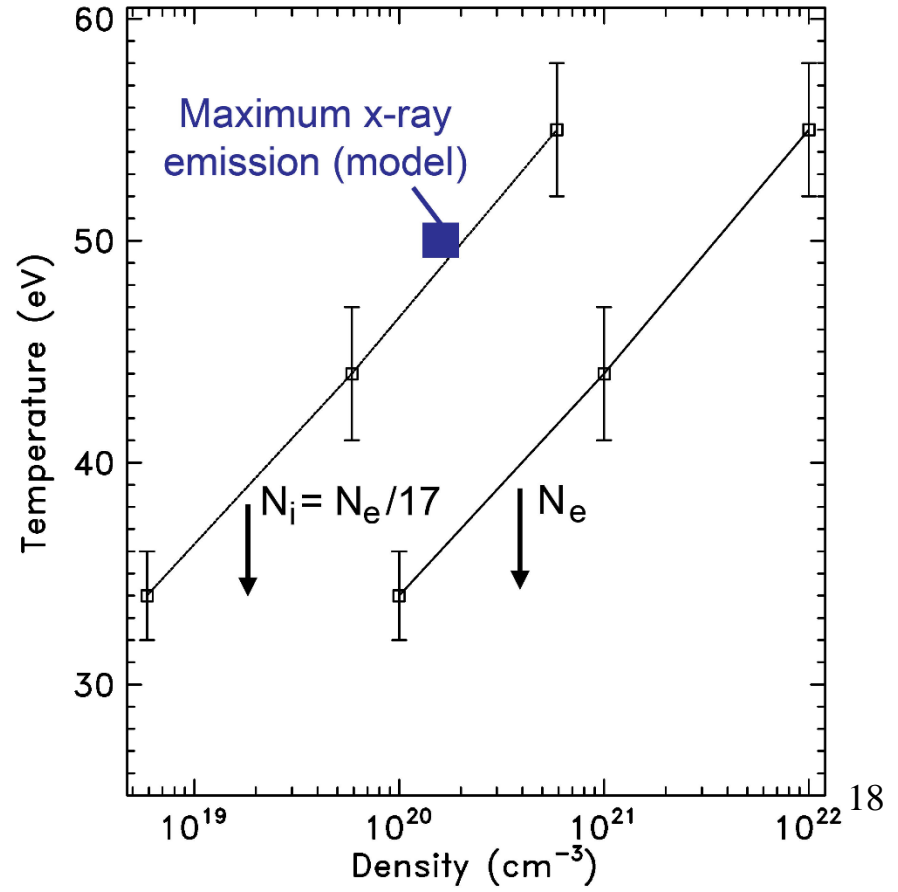
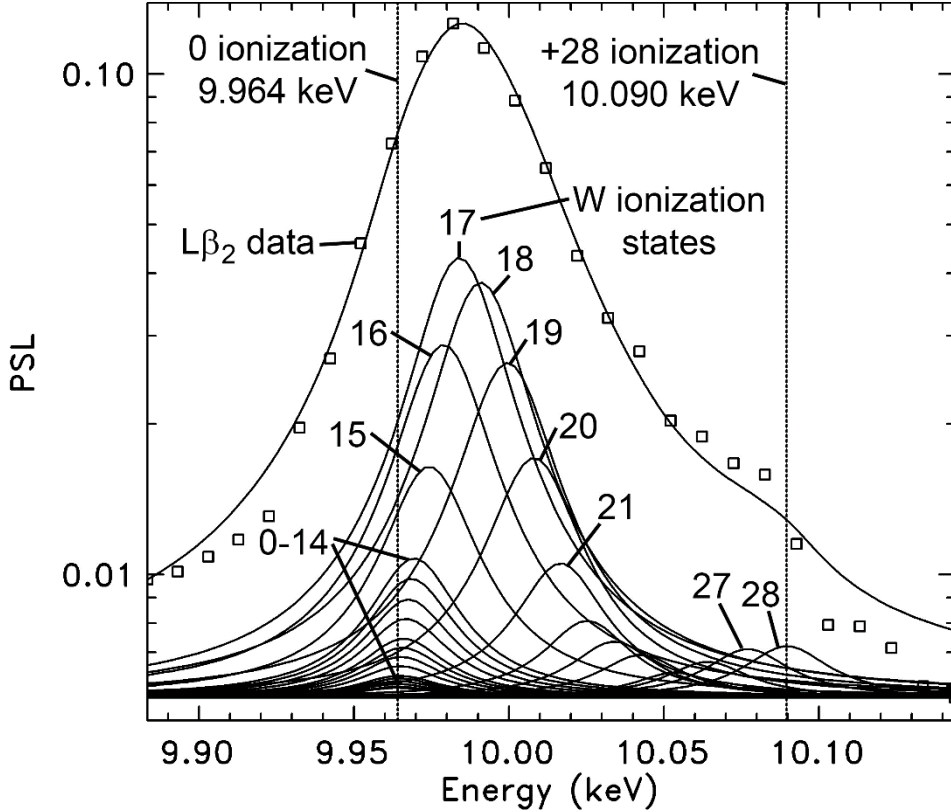
| Identification | Levels | W L Transitions | | |
|----------------|--------|---------------------|------------|-----------|
| | | Transition | Energy(eV) | Intensity |
| $L\alpha_2$ | L3M4 | $2p_{3/2}-3d_{3/2}$ | 8335.3 | 11.22 |
| $L\alpha_1$ | L3M5 | $2p_{3/2}-3d_{5/2}$ | 8398.2 | 100.00 |
| $L\eta$ | L2M1 | $2p_{1/2}-4s_{1/2}$ | 8724.4 | 1.17 |
| $L\beta_4$ | L1M2 | $2s_{1/2}-3p_{1/2}$ | 9525.2 | 3.56 |
| $L\beta_6$ | L3N1 | $2p_{3/2}-4s_{1/2}$ | 9608.2 | 1.10 |
| $L\beta_1$ | L2M4 | $2p_{1/2}-3d_{3/2}$ | 9672.6 | 55.60 |
| $L\beta_3$ | L1M3 | $2s_{1/2}-3p_{3/2}$ | 9818.9 | 5.05 |
| $L\beta_2$ | L3N5 | $2p_{3/2}-4d_{5/2}$ | 9964.1 | 22.72 |
| $L\beta_7$ | L3O1 | $2p_{3/2}-5s_{1/2}$ | 10129.2 | 1.61 |
| $L\beta_5$ | L3O5 | $2p_{3/2}-5d_{5/2}$ | 10200.4 | 0.50 |
| $L\beta_9$ | L1M5 | $2s_{1/2}-3d_{5/2}$ | 10290.7 | 0.10 |
| $L\gamma_5$ | L2N1 | $2p_{1/2}-4s_{1/2}$ | 10948.9 | 0.10 |
| $L\gamma_1$ | L2N4 | $2p_{1/2}-4d_{3/2}$ | 11286.0 | 10.45 |
| $L\gamma_6$ | L2O4 | $2p_{1/2}-5d_{3/2}$ | 11538.7 | 0.40 |
| $L\gamma_2$ | L1N2 | $2s_{1/2}-4p_{1/2}$ | 11610.5 | 1.10 |
| $L\gamma_3$ | L1N3 | $2s_{1/2}-4p_{3/2}$ | 11680.5 | 1.61 |
| $L\gamma_{11}$ | L1N5 | $2s_{1/2}-4d_{5/2}$ | 11861.9 | 0.10 |
| $L\gamma_4$ | L1O3 | $2s_{1/2}-5p_{3/2}$ | 12063.4 | 0.10 |

L-Shell Transition Energies are Accurately Calculated

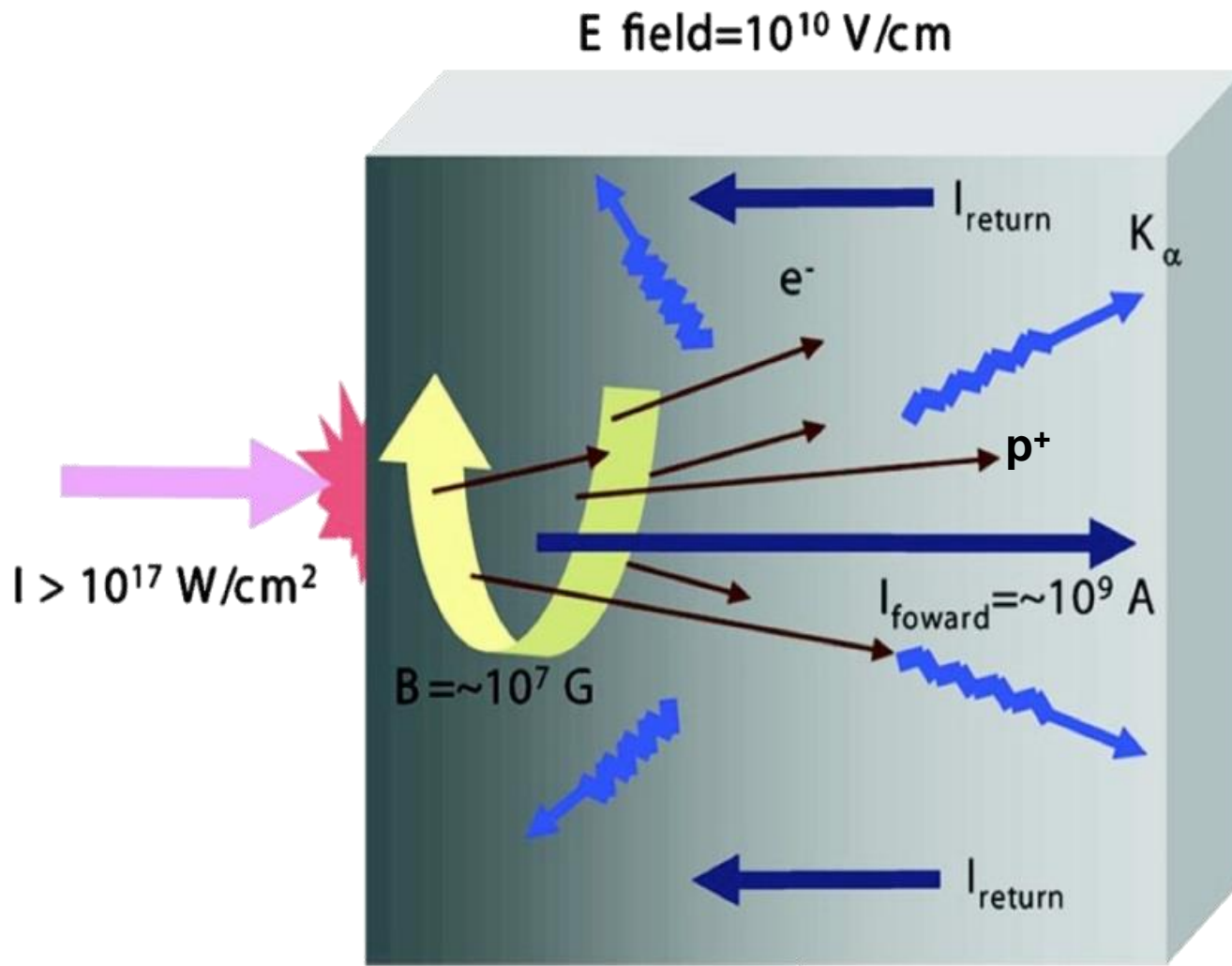
Modified Grant MCDF code (Polasik, Słabkowska, *et al.*) calculates the W L-shell transition energies with few eV absolute accuracy, and transition energy differences have eV accuracy.



Measured Ionization is used to Determine Temperature and Density

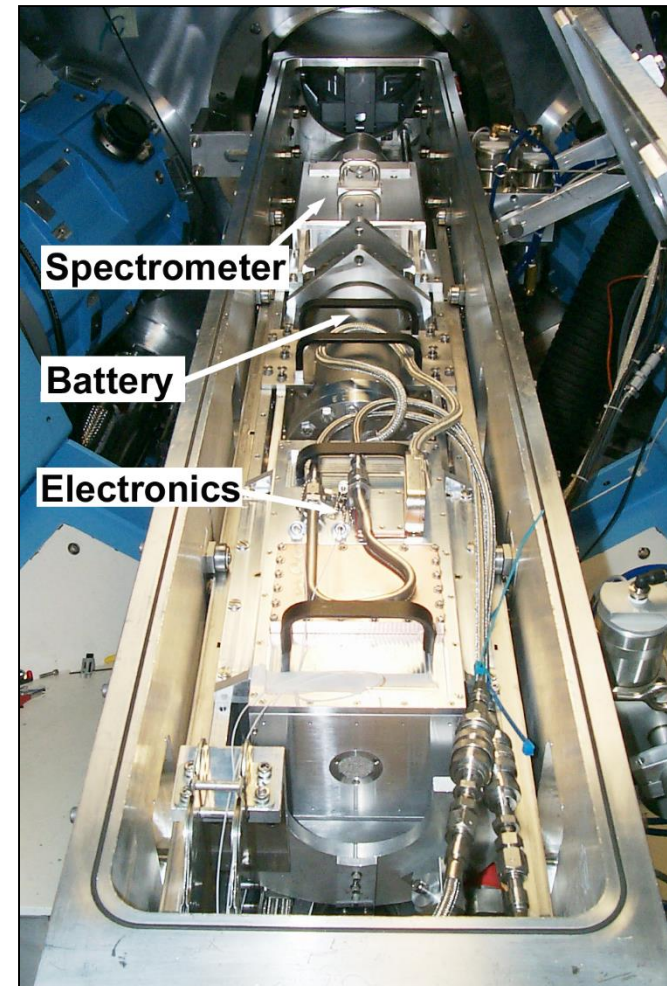
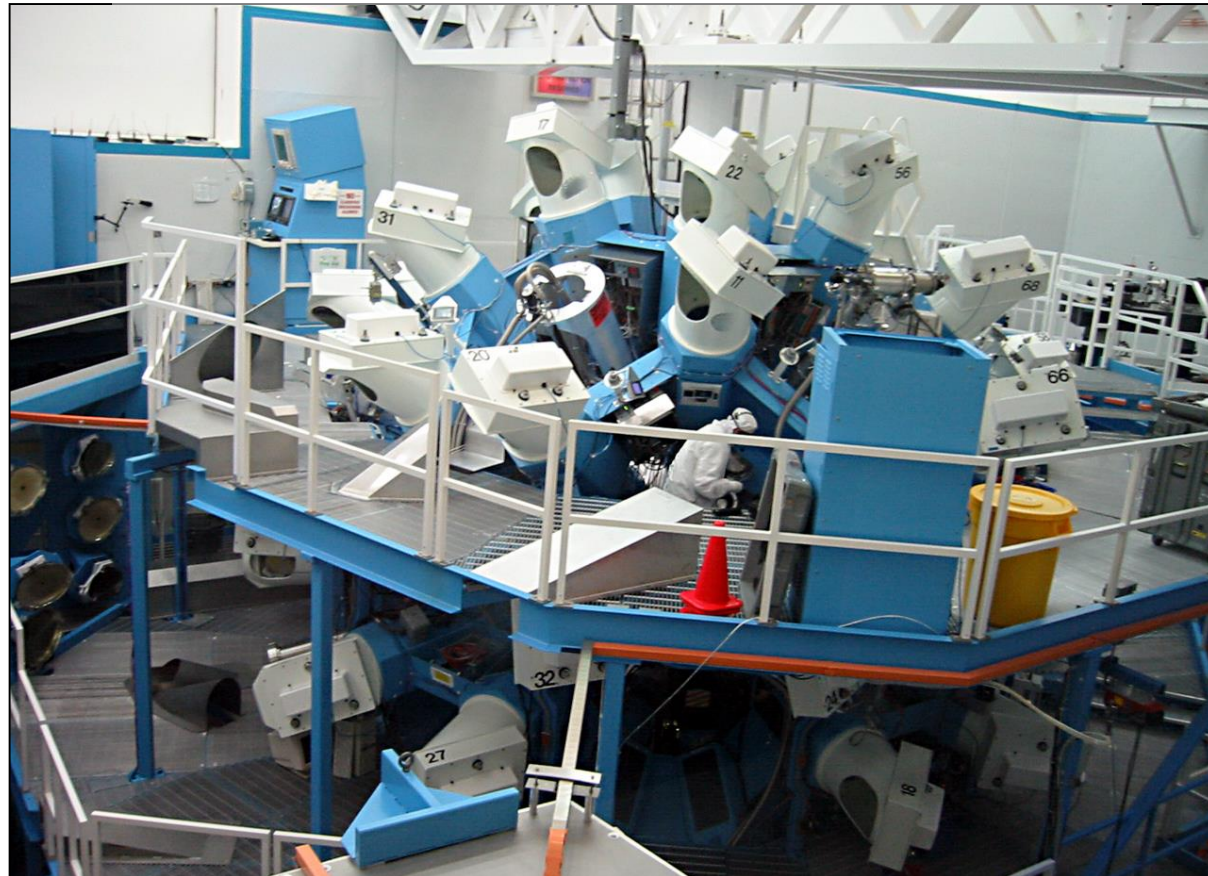


Intense Lasers Create Energetic Electrons, Positrons, Protons, X-Rays/Gammas, Strong Magnetic Fields, Etc.



Omega Laser at the Laboratory for Laser Energetics (LLE) Rochester, NY, USA

60 laser beams, 40 kJ, few ns

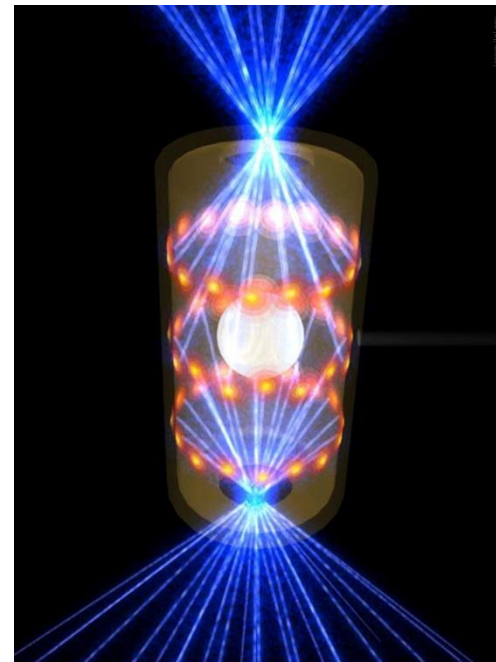


National Ignition Facility (NIF) Lawrence Livermore National Laboratory (LLNL)

196 laser beams, 1.6 MJ, few ns

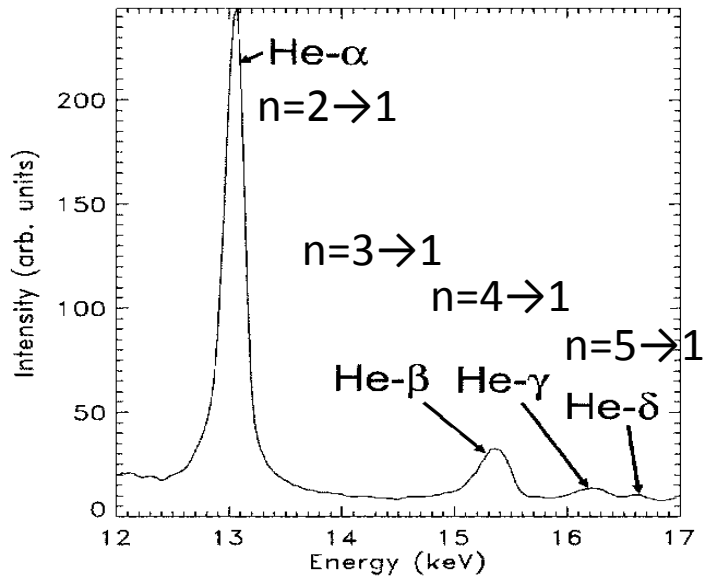
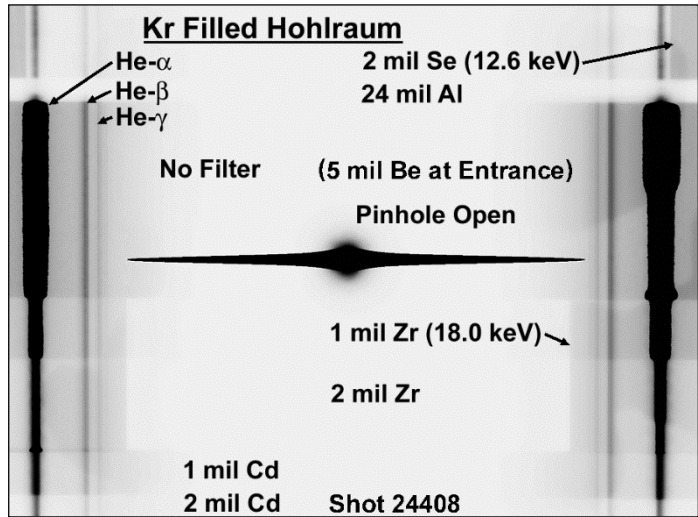


Capsule in hohlraum:



Kr K-Shell Spectra at Omega

Kr filled hohlraum



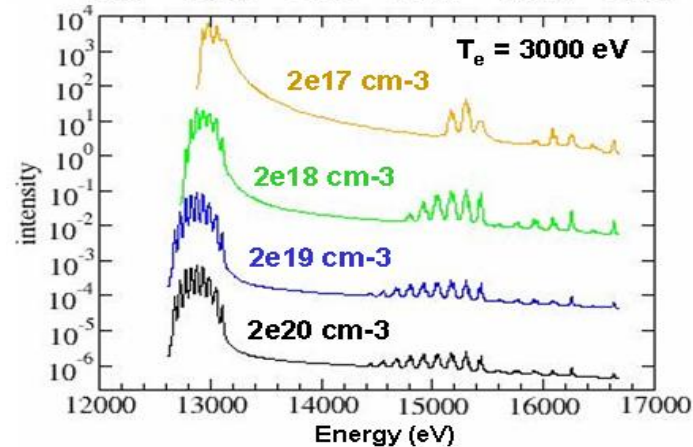
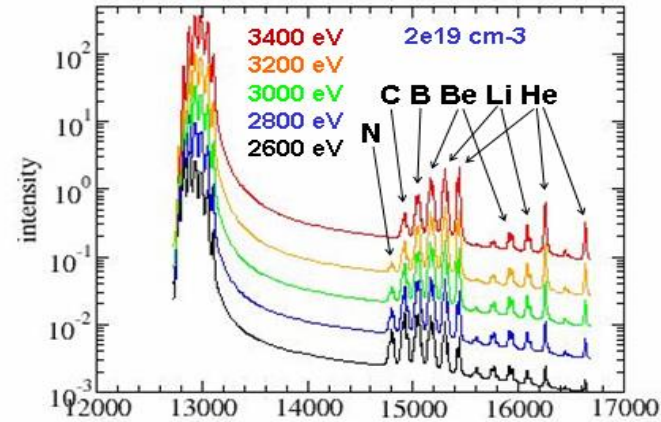
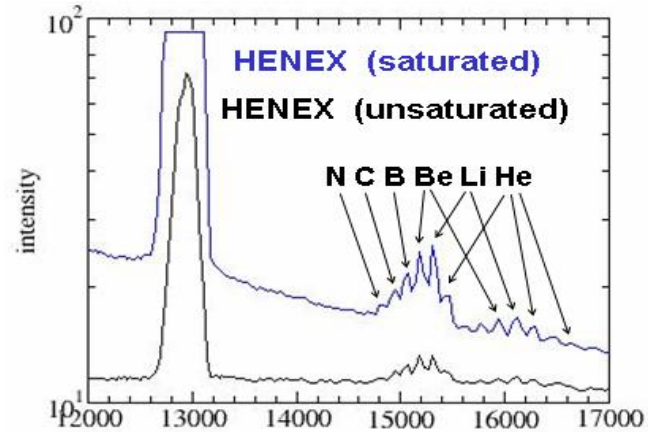
Kr filled gasbag
(bulk heating, no super-thermal electrons)

Experimental spectrum

FLYCHK by H.-K. Chung:

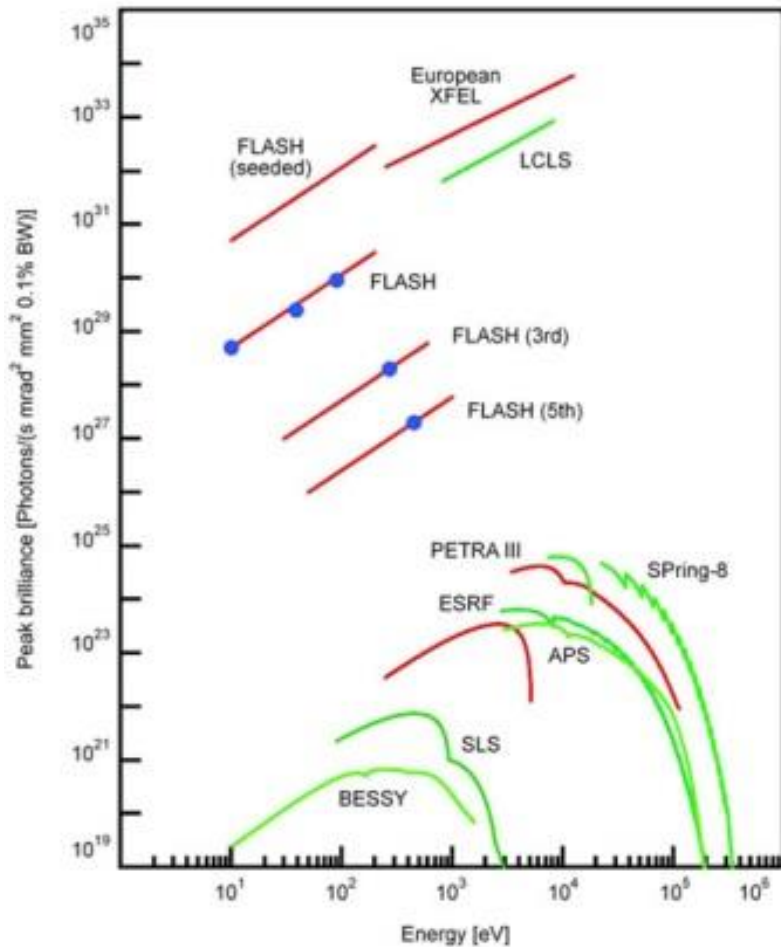
$$T_e = 2.6 \text{ keV}$$

$$N_e = 2 \times 10^{18} \text{ cm}^{-3}$$

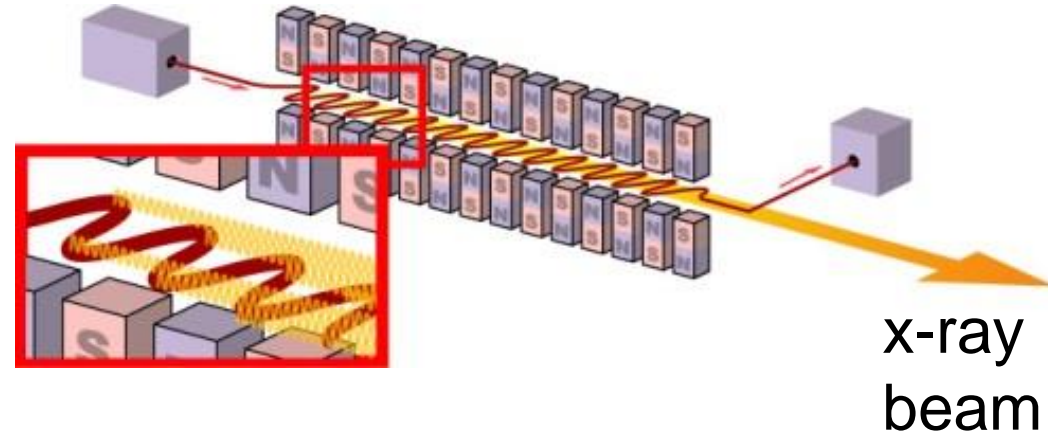


X-Ray Free Electron Laser (XFEL)

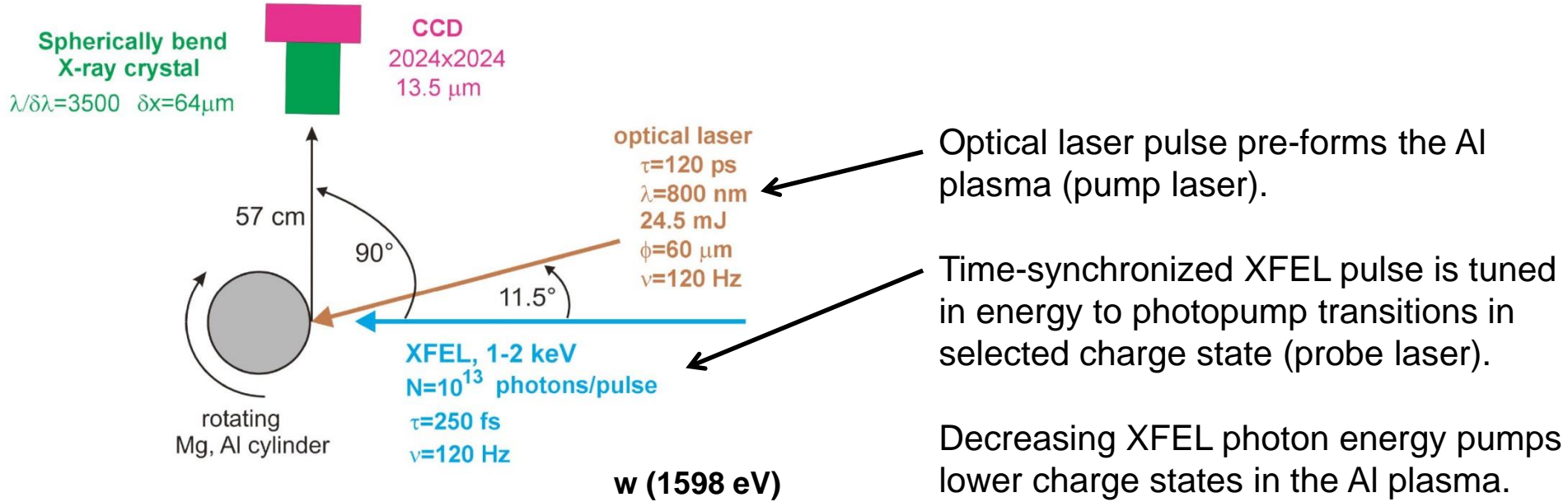
Bright, coherent, short duration, narrow bandpass, tunable energy.



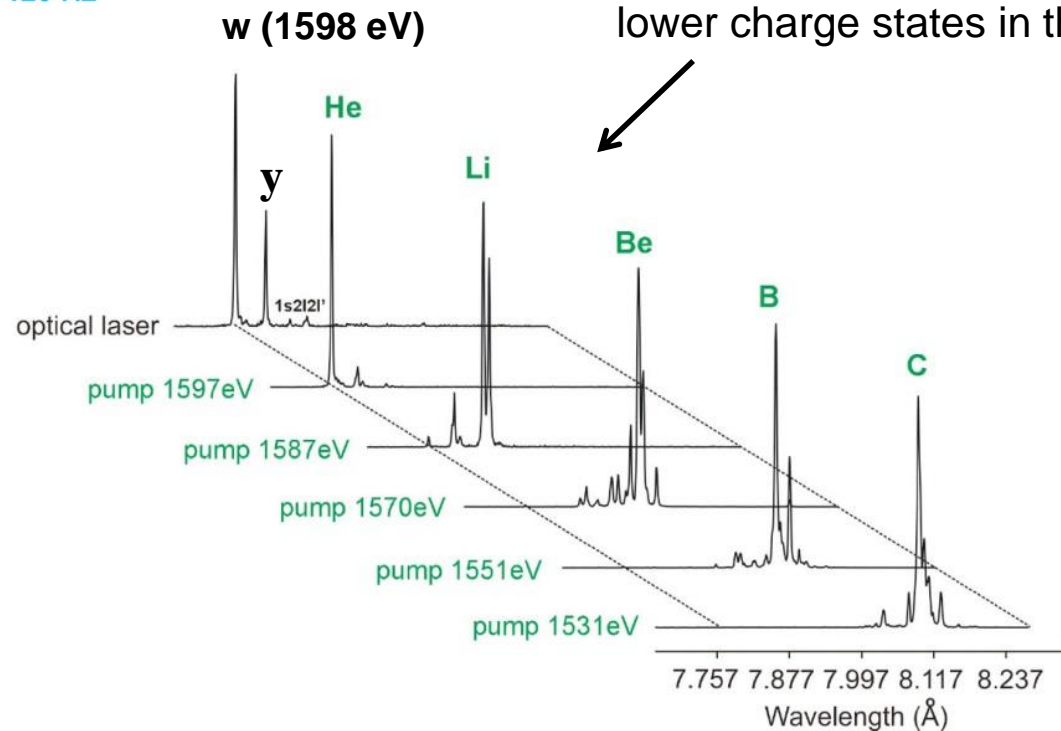
Electron bunches in undulator



Photopumping Selected Transitions in an Aluminum Plasma



F. Rosmej
 D. Lee
 J. Seely
 E. Galtier
 O. Renner
 LCLS Staff
 Yuri Ralchenko

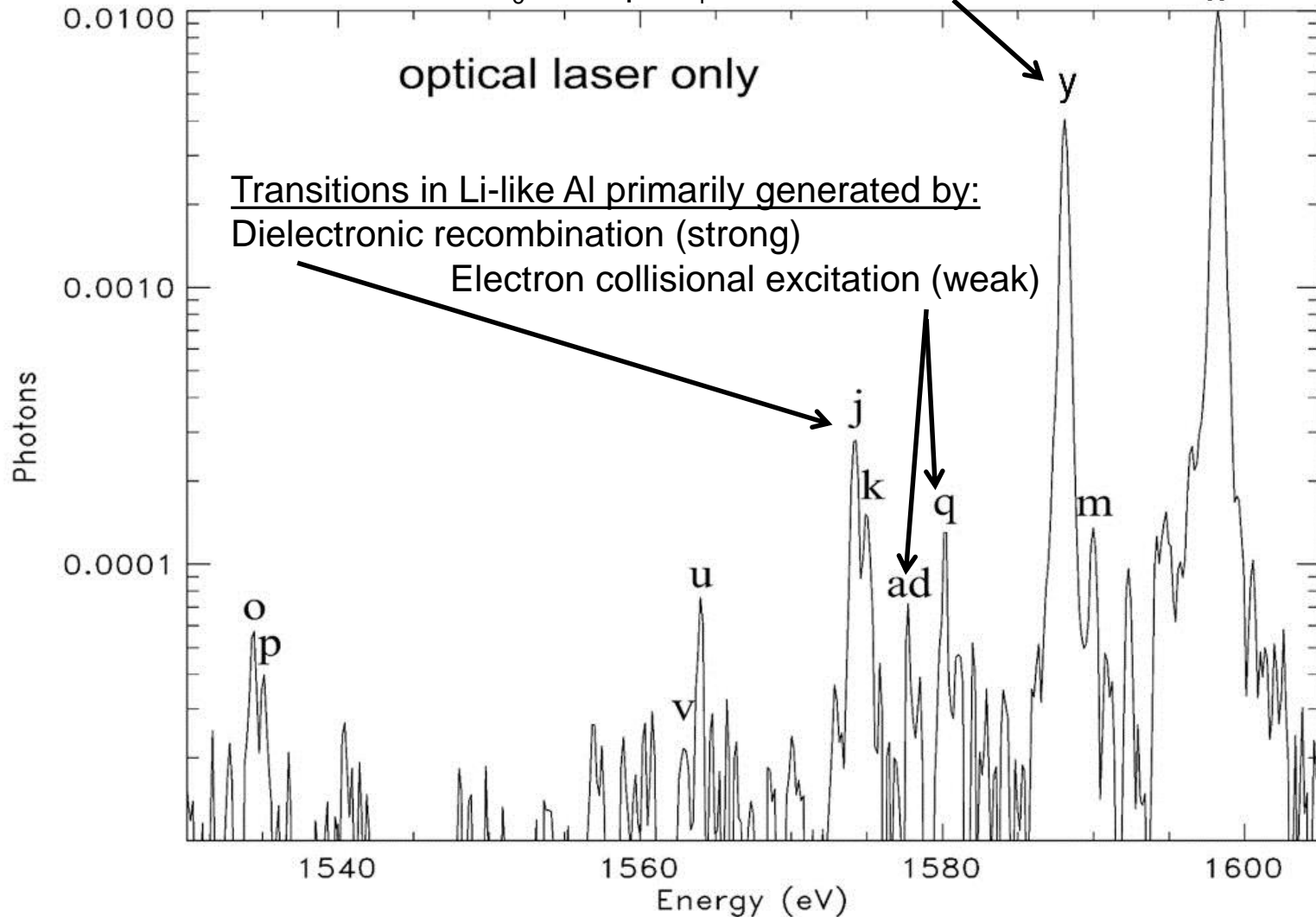


Emission Produced by Optical Laser Only

Transitions in He-like Al:

$1s^2\ ^1S_0 - 1s2p\ ^1P_1$ Resonance line

$1s^2\ ^1S_0 - 1s2p\ ^3P_1$ Intercombination line

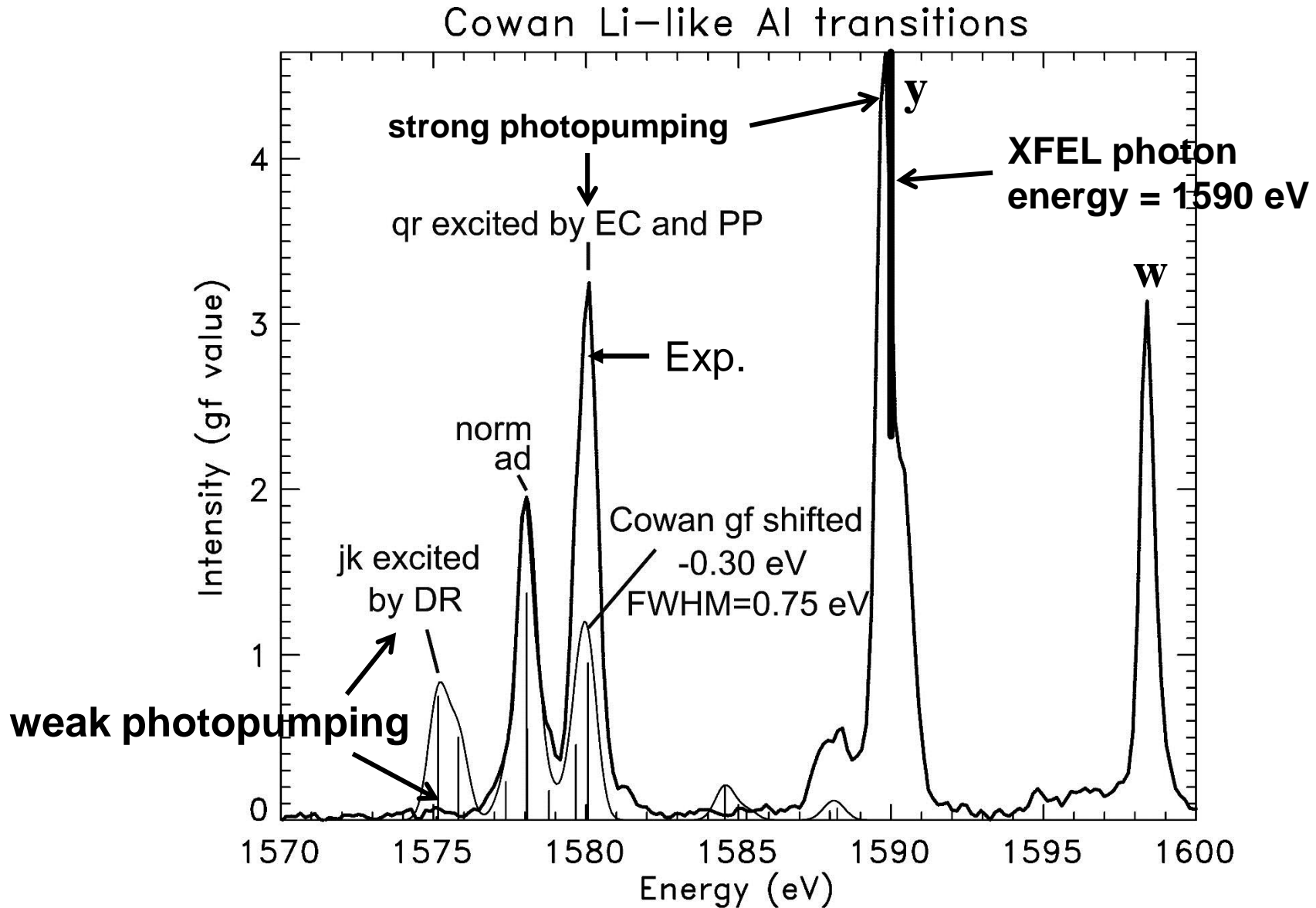


Satellites to the He-like Resonance Line

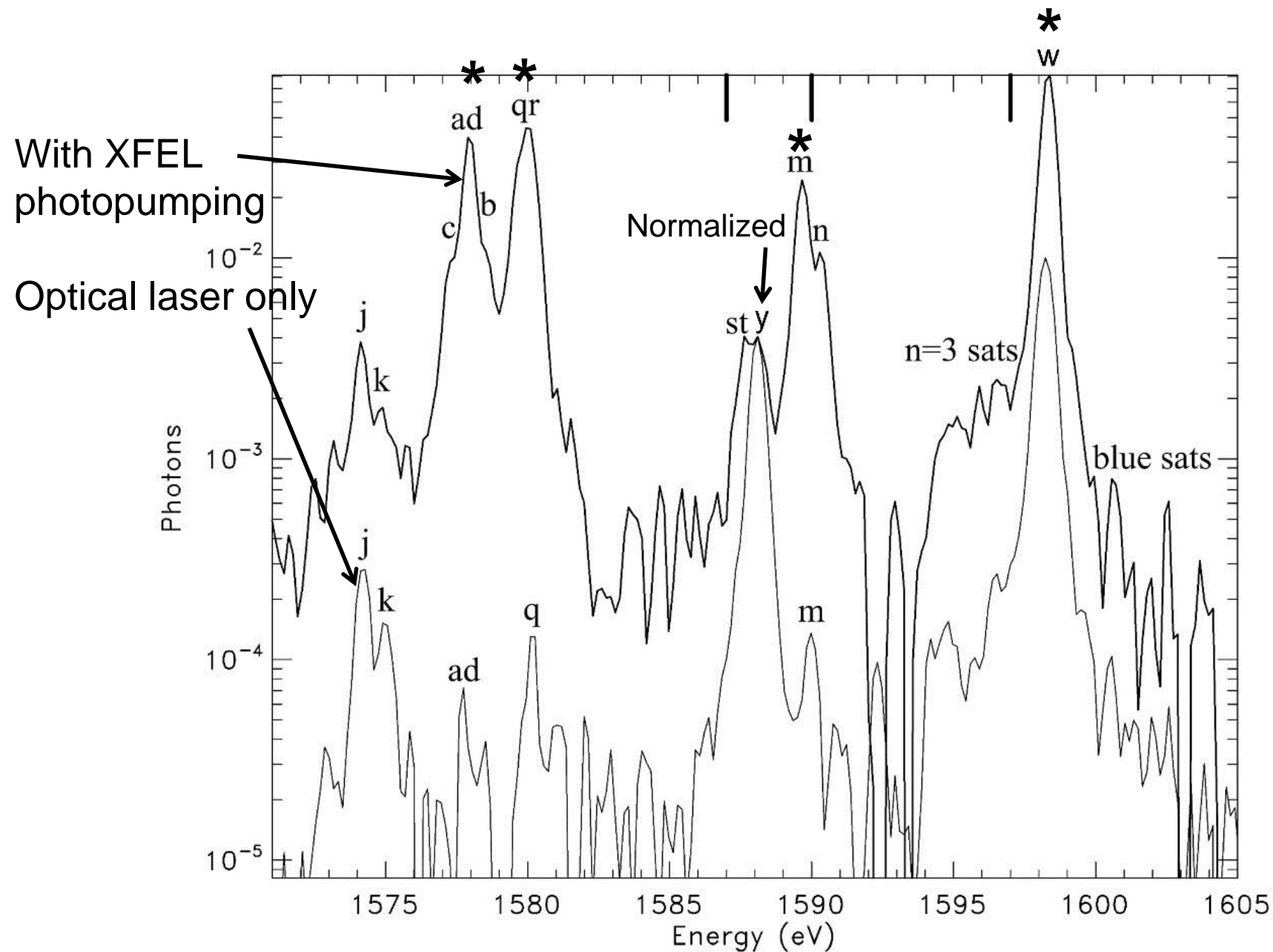
Li-like transitions from doubly-excited states.

| Array | Multiplet | Line | Key letter | | |
|----------------------|------------------|-------------------------------|------------|--|---------------------------------|
| $1s^2 2p - 1s 2p^2$ | $2P^0 - 2P$ | $1\frac{1}{2} - 1\frac{1}{2}$ | a | | Electron collisional excitation |
| | | $\frac{1}{2} - 1\frac{1}{2}$ | b | | |
| | | $1\frac{1}{2} - \frac{1}{2}$ | c | | |
| | | $\frac{1}{2} - \frac{1}{2}$ | d | | |
| | $2P^0 - 4P$ | $1\frac{1}{2} - 2\frac{1}{2}$ | e | | Dielectronic recombination |
| | | $1\frac{1}{2} - 1\frac{1}{2}$ | f | | |
| | | $\frac{1}{2} - 1\frac{1}{2}$ | g | | |
| | | $1\frac{1}{2} - \frac{1}{2}$ | h | | |
| | $2P^0 - 2D$ | $\frac{1}{2} - \frac{1}{2}$ | i | | Electron collisional excitation |
| | | $1\frac{1}{2} - 2\frac{1}{2}$ | j | | |
| | | $\frac{1}{2} - 1\frac{1}{2}$ | k | | |
| | | $1\frac{1}{2} - 1\frac{1}{2}$ | l | | |
| $1s^2 2p - 1s 2s^2$ | $2P^0 - 2S$ | $1\frac{1}{2} - \frac{1}{2}$ | m | | He-like transitions |
| | | $\frac{1}{2} - \frac{1}{2}$ | n | | |
| $1s^2 2s - 1s 2p 2s$ | $2S - (1P) 2P^0$ | $1\frac{1}{2} - \frac{1}{2}$ | o | | Electron collisional excitation |
| | | $\frac{1}{2} - 1\frac{1}{2}$ | p | | |
| | $2S - (3P) 2P^0$ | $\frac{1}{2} - 1\frac{1}{2}$ | q | | |
| | | $\frac{1}{2} - \frac{1}{2}$ | r | | |
| | $2S - 4P^0$ | $\frac{1}{2} - 1\frac{1}{2}$ | s | | |
| | | $\frac{1}{2} - \frac{1}{2}$ | t | | |
| $1s^2 - 1s 2p$ | $1S - 1P^0$ | $0 - 1$ | u | | He-like transitions |
| | $1S - 3P^0$ | $0 - 2$ | v | | |
| $1s^2 - 1s 2s$ | $1S - 3S$ | $0 - 1$ | w | | He-like transitions |
| | | $0 - 1$ | x | | |
| | | $0 - 1$ | y | | |
| | | $0 - 1$ | z | | |

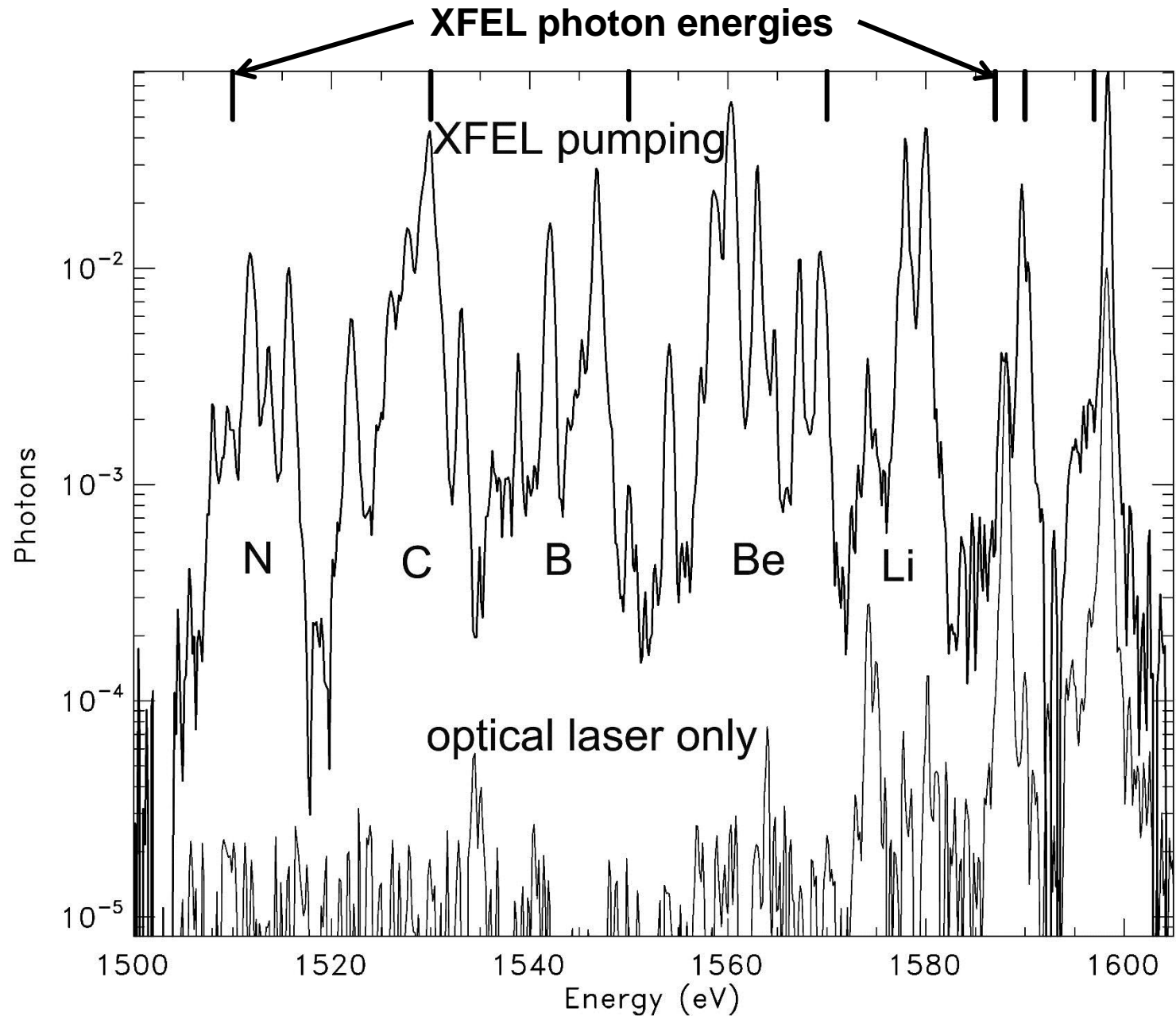
Transitions Photopumped by 1590 eV XFEL



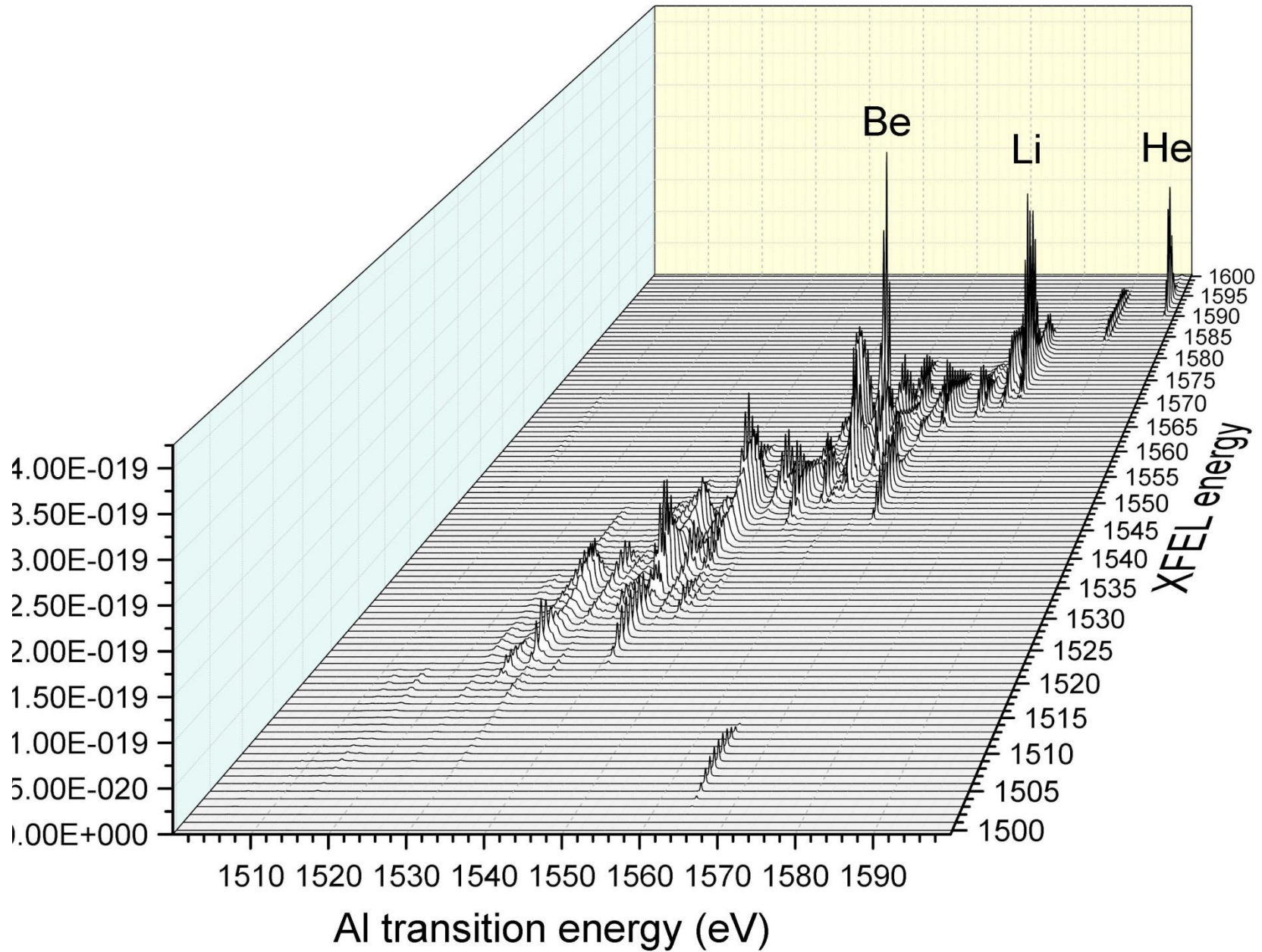
Transitions with Large Oscillator Strengths are Selectively Photopumped



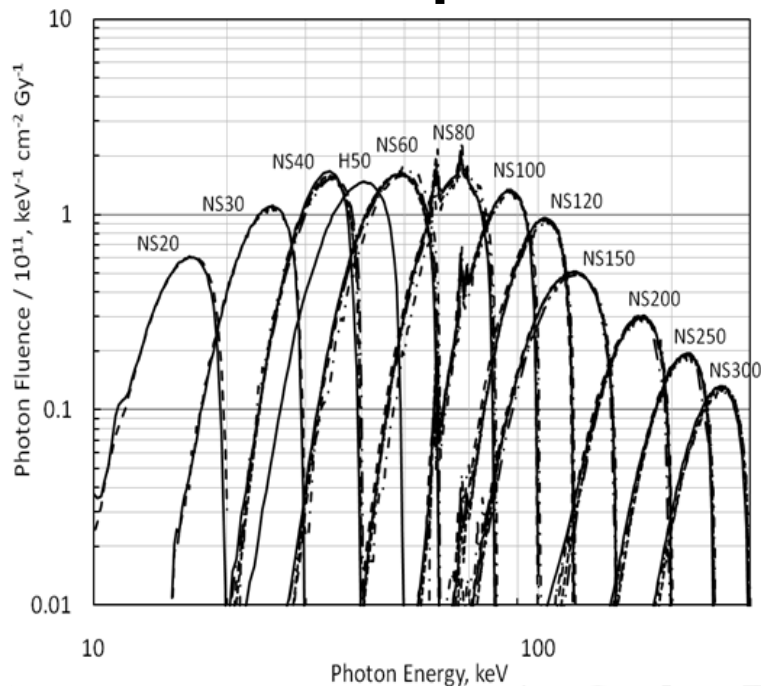
Composite Photopumped Transitions



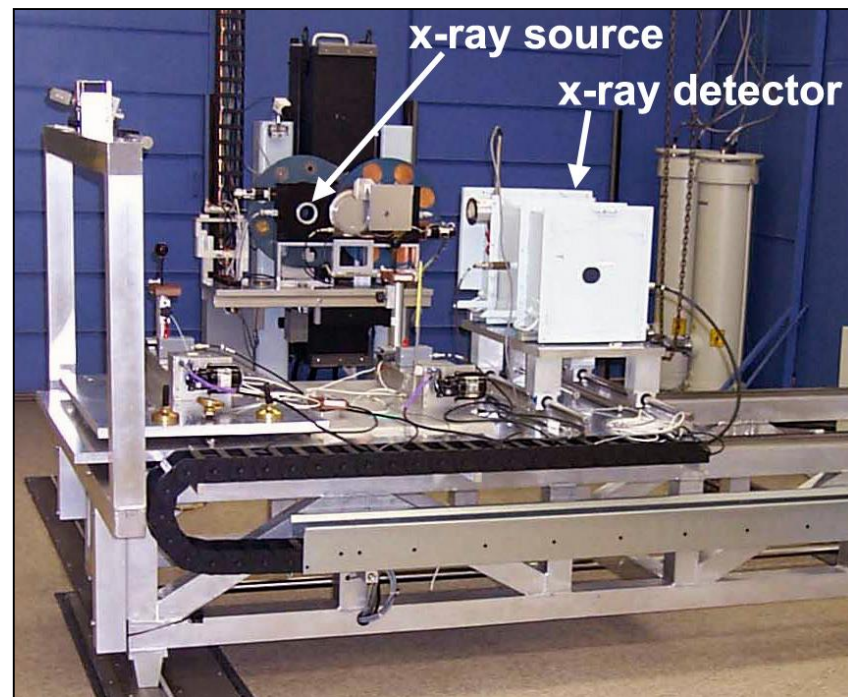
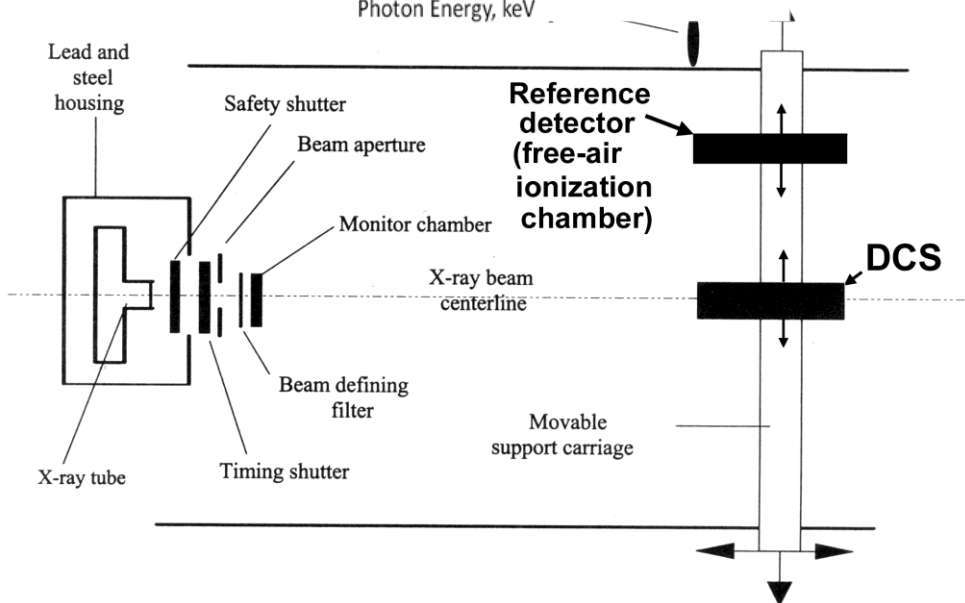
Ralchenko NOMAD Code



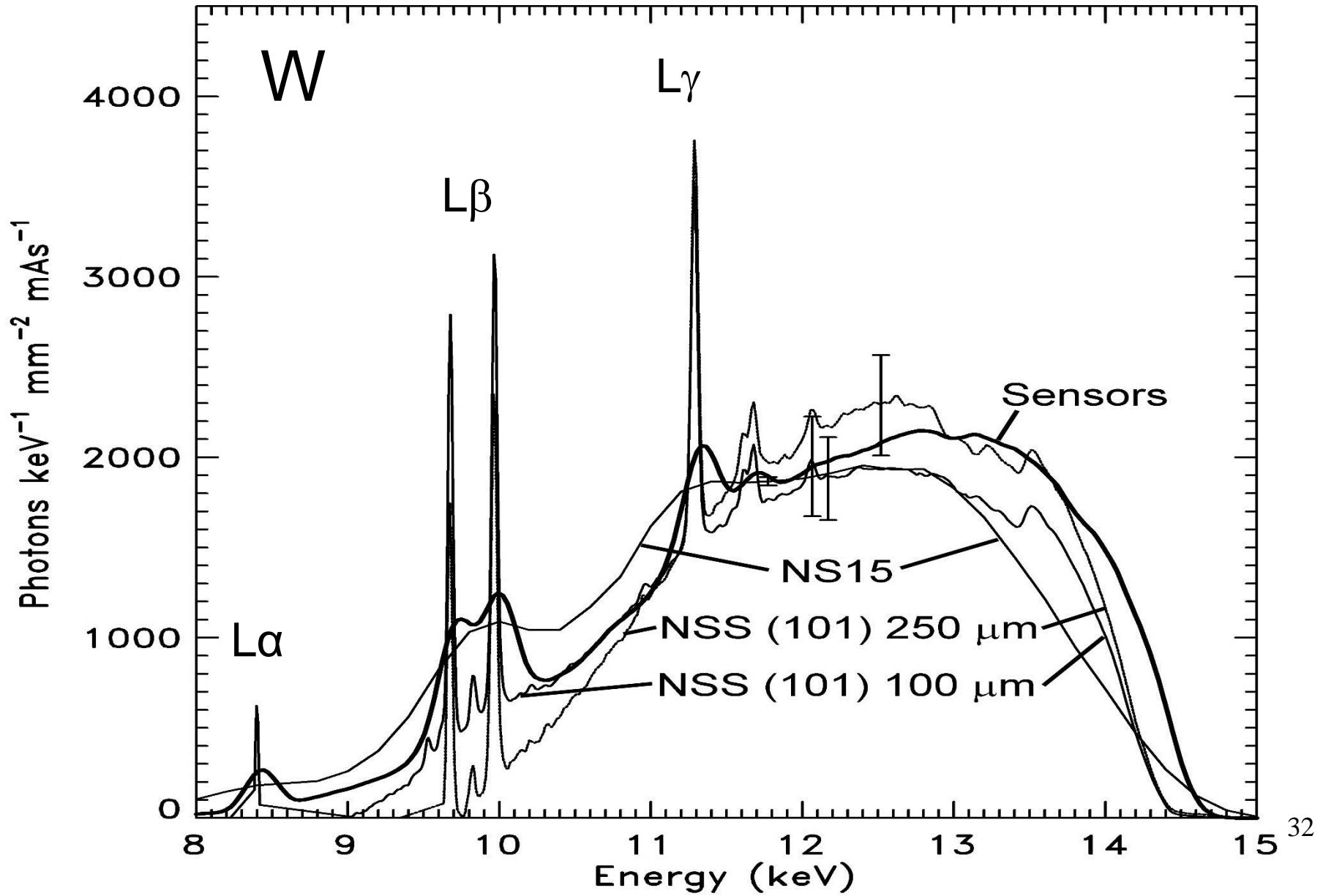
Spectrometer Calibrations (NIST)



- Calibrated x-ray fluences in energy bandpasses.
- Spectrometer signal is related to the source fluence.
- Provides instrument sensitivity calibration.



Different Calibrated Instruments Measure the Same Source Fluence (within about 13% experimental uncertainty)



Experimental X-Ray Spectroscopy: Part 2

We will use the skills you have learned this week to analyze this spectrum:

